HOWARD UNIVERSITY

High Temperature Superconductivity in Praseodymium Doped(0 %, 2 %, 4 %) in Melt-Textured $Y_{1-x}Pr_xBa_2Cu_3O_{7-\delta}$ Systems.

*

A Thesis
Submitted to Faculty of the
Graduate School of Arts and Sciences

of

Howard University
in partial fulfillment of
the requirement for the
degree of

Master of Science

Department of Physics and Astronomy

by

Claudell James

*

Washington, D.C.
August 1995

Howard University
Graduate School of Arts and Sciences
Department of Physics

Thesis Committee

Robert Catchings, Ph. D.

Prabhakar Misra, Ph. D.

Arthur N. Thorpe, Ph. D.

Arthur N. Thorpe, Ph.D
Thesis Advisor

Candidate: Claudell James

Date of Defense: July 19, 1995

DEDICATION

This Thesis is Dedicated
to
Susan Lea James

ACKNOWLEDGEMENTS

The author wishes to express his sincere gratitude to his thesis advisor and mentor, Dr. Arthur N. Thorpe, for suggesting this subject and for helpful criticism and advice throughout its investigation. The author also wishes to express his thanks to Mr. Shouxiang Hu, of the Catholic University, for fabricating the samples used for this study.

The author is especially indebted to David D. Davis for the extensive time spent in assisting with the operation of the experiment's equipment and the computer software; and I thank, wholeheartedly, the assistance given by Julius Grant in computer operation and editing of this thesis.

ABSTRACT

A study of the magnetic and structural properties of the alloy $Y_{1-x}Pr_xBa_2Cu_3O_{7-\delta}$ of 0%, 2%, and 4% doping of praseodymium is presented. The resulting oxides of the alloy series are a high-temperature superconductor Y-Ba-Cu-O, which has an orthorhombic superconducting crystal-lattice. Magnetic relaxation studies have been performed on the Y-Pr-Ba-Cu0 bulk samples for field orientation parallel to the c-axis, using a vibrating sample magnetometer. Relaxation was measured at several temperatures to obtain the irreversible magnetization curves used for the Bean model.

Magnetization current densities were derived from the relaxation data. Field and temperature dependence of the logarithmic flux-creep relaxation was measured in critical state. The data indicates that the effective activation energy U_{eff} increases with increasing T between 77 K and 86 K. Also, the data shows that $U_{eff}(T)$ and superconducting transition temperature, Tc, decreased as the lattice parameters increased with increasing Pr ion concentration, x, for the corresponding $Y_{1-x}Pr_xBa_xCu_3O_{7-\delta}$ oxides. One contribution to Tc decrease in this sampling is suspected to be due to the larger ionic radius of the Pr^{3+} ion. The upper critical field (H_{c2}) was measured in the presence of magnetic field parallel to the c axis. A linear temperature dependence with H_{c2} was obtained.

TABLE OF CONTENTS

LIST OF FIGURES

LIST OF TABLES

I. INTRODUCTION

Superconductivity is a phenomenon of great interest because of its unlimited technical applications that will revolutionize present methods and systems design, if the phenomena could be acquired at near room temperature. Properties that make superconductivity unique are: Its ability to maintain a current that will persist for years without decaying in a superconducting ring while exhibiting no electrical resistance and a superconductor expels applied magnetic fields so that the field is zero everywhere inside. These properties and behaviors of superconductors cannot be explained by classical physics. In the superconducting state, electrons are found to be in a quantum condensation. This quantum behavior has been measured in the superconducting ring.

The era of low temperature physics began in 1908 when the Dutch physicist Heike Kammerling Onnes first produced liquid helium, which has a boiling temperature of 4.2 K. While testing the resistivity of mercury, Hg; he found that it was zero at this temperature. He called this phenomena of perfect conductivity, *superconductivity*. This discovery lead many other elemental metals were found to exhibit zero resistance when the temperature was lowered below a certain characteristic temperature of the material called the critical temperature, Tc.

The magnetic properties of superconductors are equally difficult to explain. In 1933 W. Meissner and R. Ochsenfeld studied the magnetic behavior of superconductors

and found that when in the presence of a magnetic field a superconductor is cooled below its critical temperature all of the magnetic flux is expelled from the interior; this is called the Meissner Effect. Additionally, these materials lost their superconductive behavior above a certain temperature-dependent critical magnetic field, $B_c(T)$. The nature and origin of the superconducting state were first explained by J.Bardeen, L.N. Cooper, and J.R. Schrieffer in 1957. Central to this theory called the BCS theory, is the formation of a bond electron state called a Cooper pair. A Cooper pair, consisting of two electrons with equal and opposite momenta and opposite spins. The two electrons can form a bond state through a weak attractive interaction in which the crystal lattice serves as a mediator. In the ground state all electron form Cooper pairs, and all are in the same quantum state of zero momentum. Then the superconducting state is represented by a single coherent wave function, which extends over the entire volume of the sample. The BCS model predicts an energy gap, while for a normal conductor there is no gap.

In 1986, J. Georg Bednorz and K. Alex Muller found superconductivity at 30 K. This marked the beginning of *high temperature* superconductivity. Today that figure is as high as 125 K in complex metallic oxides, but the mechanisms responsible for superconductivity in these materials remain elusive for investigators. When the critical temperatures of some superconducting elements, classified as Type I superconductors, are measured in an applied magnetic field B, the value of Tc decreases with increasing magnetic field. When the applied magnetic field exceeds a certain critical magnetic field H_{c1}, the superconducting state is destroyed, and the material behaves like a normal conductor with finite resistance.

If the applied field exceeds the critical field at 0 K, $H_{cl}(0)$, the metal will never become superconducting at any temperature. Values for the critical field for Type I superconductors are quite low, of the order of 0.1 Tesla. Thus, Type I superconductors cannot be used to construct high field magnets for commercial use.

Looking at the physics of superconductivity, it may be shown that the magnetic field inside a superconducting sample cannot change with time. Ohm's law says the electric field in a conductor is proportional to the resistance of the conductor. Since R=0, the electric field in its interior must be zero. From Faraday's law of induction,

$$\int E \cdot ds = -d\Phi/dt. \qquad (1)$$

The line integral of the electric field E around any closed loop is equal to the negative rate of change in the magnetic flux Φ through the loop. Since E is zero everywhere inside the superconductor, the integral over any closed path is zero, hence $d\Phi/dt = 0$. The magnet flux in the superconductor cannot change. Thus, a conclusion may be drawn that B must remain constant inside the superconductor:

$$-d\Phi/dt = \int E \cdot ds \qquad (2)$$

integrate,

$$\Phi = \int 0 \, ds$$

$$BA = \text{Constant} \cdot A$$

A - area inside loop.

Thus,

$$B = \text{Constant.} \tag{3}$$

It was assumed that superconductivity was a manifestation of perfect conductivity. A perfect conductor when cooled below its critical temperature in the presence of an applied magnetic field, the field should be trapped in its interior even after the field is removed. The final state in a magnetic field depended upon which occurred first, the application of the fields or the cooling below the critical temperature. Then, W. Meissner and R. Ochsenfeld in 1933 discovered that when a metal becomes superconducting the field is actually expelled so that $B=0$ was achieved whether the field was applied before or after the material was cooled below its critical temperature. This means that not only is $d\Phi/dt=0$, but magnetic flux Φ must equal zero as well. The physics of this is as follows:

An electron of charge -e placed in an electric field feels a force -eE without frictional forces. Newton's law becomes

$$m \cdot dv/dt = -eE. \tag{4}$$

Combined with the definition of current density, $J = \rho ev$, gives

$$\partial J/\partial t = \rho e(\partial v/\partial t) \tag{5}$$

$$\partial J/\partial t = \rho e(eE/m) = \rho e^2/m \cdot E. \tag{6}$$

Since the charge carriers are Cooper pairs, e is replaced by 2e and m by 2m so

$$\partial J/\partial t = 2\rho e^2/m \cdot E. \qquad (7)$$

With an external field present, there is a current density J_e that acts as a source for that field and J_s the superconducting current density. According to the Maxwell equation the total field may be written as

$$\nabla \times B = \mu_o(J_s + J_e). \qquad (8)$$

Inside the superconductor J_s is zero, and the electric field obeys the Faraday law

$$\nabla \times E = - \partial B/\partial t. \qquad (9)$$

Combining equation (7) with (9) yields:

$$E = \partial J/\partial t \cdot m/2\rho e^2 \qquad (10)$$

$$\nabla \times \partial J/\partial t \cdot m/2\rho e^2 = - \partial B/\partial t \qquad (11)$$

Rearranged

$$\partial/\partial t(B + m/2\rho e^2 \nabla \times J_s) = 0. \qquad (12)$$

A perfect conductor obviously requires only that the quantity in parentheses be constant in time; but this still causes the field in the interior of the superconductor to be constant in time rather than to vanish as the Meissner effect requires. London proposed a more restrictive equation for superconductors. Which is

$$B + m/ 2\rho e^2 \nabla \times J_s = 0. \qquad -(13)$$

J_s can be expressed in Equation (E).

$$J_s = \nabla \times B/\mu_o \qquad (14)$$

and

$$B + m/2\rho e^2 \nabla \times J_s = 0 \qquad (15)$$

$$B + m/2\rho e^2 \nabla \times (\nabla \times B) = 0. \qquad (16)$$

Using the identity

$$\nabla \times (\nabla \times B) = \nabla(\nabla \cdot B) - \nabla^2 B/\mu_o \qquad (17)$$

Another Maxwell equation has $\nabla \cdot B = 0$, thus

$$B + m/2\rho e^2(-\nabla^2 B) = 0, \qquad (18)$$

and writing as

$$B = \lambda^2 \nabla^2 B, \tag{19}$$

where

$$\lambda^2 = m/2\mu_o \rho e^2. \tag{20}$$

In the case of a semi-infinite block with a face at x = 0, with the external field B in the z direction, parallel to the face of the block, only B in the x-direction varies so that B equation above can be solved

$$B(x) = \lambda^2 \, d^2B(x)/dx^2. \tag{21}$$

The solution has B = constant on the boundary at x = 0, while x>0, inside the superconductor, the solution to this second order differential equation is

$$d^2B(x)/dx^2 - B(x)/\lambda^2 = 0 \tag{22}$$

solving

$$B(x) = B(0)e^{-x/\lambda}. \tag{23}$$

We see that the field decays exponentially as it penetrates into the superconductor and vanishes in the interior. On the surface there is a field that extends approximately the penetration depth λ into the superconductor.

Then a superconductor is a perfect conductor and perfect diamagnet; it has no magnetic flux inside (B=0). B=0 in a superconductor is as fundamental as the property of zero resistance. When a magnetic field is sufficiently large, the

superconducting state will be destroyed and the field will completely penetrate the entire sample. The resistance will then go from zero to the value known for a normal conductor. Being a perfect diamagnet (B=0 inside), a superconductor will repel a permanent magnet, just as an electrical conductor expels static electrical fields to its surface, thereby canceling the externally applied field inside the conductor.

There exists superconducting materials characterized by two critical magnetic fields, designated as B_{c1} and B_{c2}; these are called Type II superconductors. If the applied field is less than B_{c1}, the material is entirely superconducting and there is no flux penetration, just as with the Type I materials. If the field exceeds the upper critical field B_{c2}, the flux penetrates completely and the superconducting state is destroyed. For fields between B_{c1} and B_{c2}, the material is in a mixed state, called the vortex state. In the vortex state, the material can have zero resistance and have partial flux penetration. The values of the critical fields are very large for Type II superconductors compared with Type I superconductors(Table 1). Thus, Type II superconductors are well suited for constructing high-field superconducting magnets.

With the discovery of high temperature superconducting oxide La-Sr-Cu-O in 1986 having a critical temperature (Tc) of 35 K, and in 1987, the discovery of Y-Ba-Cu-O with a Tc of 92 K, and much higher B_{c2} (Table 2), there has been intense research in the field of high temperature superconductivity, since it became possible to use liquid nitrogen (liquefies at 77.4 K) refrigeration, which is easier to use and much less costly than the use of liquid helium (liquefies at 4.2 K). $Y_1Ba_2Cu_3O_{7-\delta}$(called 123) materials have maintained the greatest interest of study among many copper oxide-based superconductors.

Table 1 (*Superconductivity supplement for Physics*, Serway, 1988).

Critical Temperatures and critical magnetic fields (T = 0 K) sample of Type I and Type II Superconductors with their upper critical magnetic field.

Superconductor(Type I)	Tc(K)	$B_{c1}(0)$ in Tesla
Al	1.180	0.0105
Ga	1.083	0.0058
Hg	4.153	0.0411
In	3.408	0.0281
Pb	7.193	0.0803
Sn	3.722	0.0305
Zn	0.85	0.0054
Superconductor(Type II)		$B_{c2}(0)$ in Tesla.
Nb_3Al	18.7	32.4
Nb_3Ge	23.0	38.0
NbN	15.7	15.3
$Nb_3(AlGe)$	21.0	44.0
PbMoS	14.4	60.0

The practical applications of HTSC superconductors are contingent upon achieving high critical current at high Tc. The upper value of has been in the range of 2.3×10^8 A/cm^2 at 0 K. Current density decreases immensely under applied fields,

which makes practical applications to commercial use difficult. Another area of study is in HTSC superconductor's anisotropic crystal structure, which limits current densities in bulk polycrystalline materials. The melt-processing techniques used to make the samples of this study has made progress in eliminating intergranular and high angle boundaries of these polycrystalline compounds that are destructive to current density and decreasing Tc.

Table 2 (*Superconductivity supplement for Physics* , Serway, 1988).
Critical temperatures and upper critical field H_{c2} of some HTSC materials in bulk crystalline form.

Superconductor	Tc(K)	$H_{c2}(0)$ in Tesla
La-Ba-Cu-O	30	>36
$La_2Cu_3O_7$	40	>36
$YBa_2Cu_3O_7$	95	80 - 320
Bi-Sr-Ca-Cu-O	120	>28
Ti-Ba-Ca-Cu-O	125	28

Nevertheless, large relaxation effects causing a decay of the magnetization are observed due to a thermally activated process that results from a combination of low pinning potentials and high temperatures. This relaxation effect is called **flux creep.** Essentially, flux creep is where trapped-flux lines jump from one pinning area to

another. Flux creep reaction distances (coherence lengths) are of the order of 10 Å; making them unstable and thus migration takes place easily. In principle, the creep rate can be decreased by increasing the pinning potential; the methods of increasing pinning potential are the source of intense investigation. Improvement in pinning is expected to occur if defects or doping materials are introduced that are of the sizes of the coherence length, within the material. This in turn makes it possible to increase the current density flow, Jc, in bulk polycrystalline YBCO superconductors by eliminating the large weak links and cracks and aligning the crystal structure, thereby slowing the decrease in transition temperature, Tc, slope.

The $Y_{1-x}Pr_xBa_2Cu_3O_{7-\delta}$ (YPrBCO) system is appealing for its use in investigating and attempting to understand the depression of transition temperature, Tc, with increasing Pr concentration x. Investigations for $x=0.1$ to $x=1.0$ with praseodymium, has revealed a structure that remains orthorhombic throughout the solid solution range $0 \leq x \leq 1.0$. The total oxygen content remained essentially constant at 6.95 ± 0.03 per formula unit, indicating that the superconducting in the system is dictated solely by the Pr ion content[1]. This thesis will continue investigating for bulk samples of x=0 %, 2 %, and 4 % praseodymium per unit cell, to observe the effects of small concentration on the superconductivity.

Experiments with $Y_{1-x}Pr_xBa_2Cu_3O_{1-\delta}$ compounds have shown that the transition temperature gradually falls from about, 90 K at x=0 to 0 K at $x \approx 0.55$ in praseodymium, where the superconductivity disappears[2,3](fig. 1). There are two suggestions for this behavior: First some behavior that allows the filing of mobile holes in the conducting CuO_2 planes by electrons donated by the introduction of Pr ions

with a valence greater than +3, which is the valence of the Y ions[4-6]. Other studies: Magnetic-susceptibility[6,7], Hall-effect[8], thermoelectric-power[9], muon-spin resonance(USR)[10], and neutron diffraction[11], were consistent with a Pr valence considerably larger than +3. The second possible behavior suppressing Tc, is a possibility that the Cooper pairs are being broken apart due to spin-dependent exchange scattering of mobile holes in the CuO_2 valence band by Pr ions[12-16]. Since the Pr ions have valences of +3 or +4 and a magnetic moment that have an affinity to couple with the spins of the holes in the conducting CuO^2 planes, this would disrupt the Cooper pairing.

This thesis, by looking at small doping concentration of Pr, has goals of exposing greater insight of the behavior of Tc suppression on YPrBCO structures. The results of a variety of experiments and comments on the overall understanding of the electronic behavior of Pr in $Y_{1-x}Pr_xBa_2Cu_3O_{7-\delta}$ are summarized in the text.

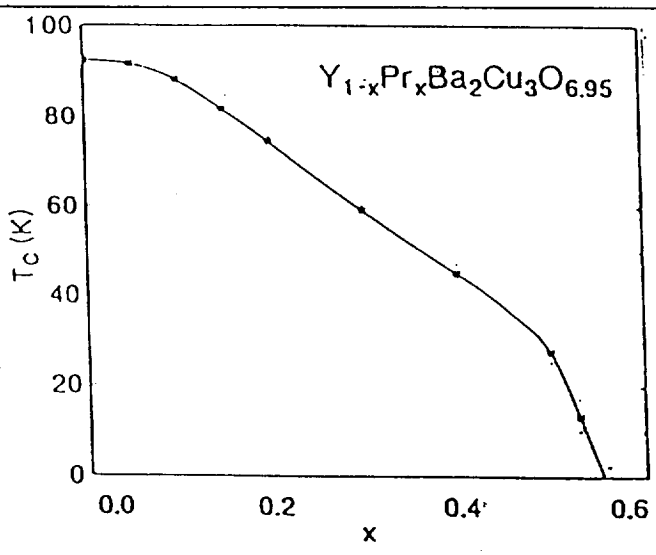

Fig. 1. Superconducting transition temperature vs. Pr concentration x.

II. THEORY

A. Magnetic Hysteresis

Magnetism in superconductors is the result of the distribution of induced supercurrents, which thereby causes magnetic field flux expulsion in the sample. In materials that allow superconducting as well as flux penetration (called Type II materials), an oscillating field can simultaneously contain sheets of oppositely directed currents at different depths in the material since surface supercurrents can shield the interior of the material from the effects of changing the applied field. Type I material does not allow this mixed phase state.

When HTSC material is subjected to an external field increasing from zero to a maximum, and then returning to zero, the direction of current induced by the initial increase may be preserved below a surface layer of reversed currents. The magnetic effects of the oppositely directed current sheets do not completely cancel, leaving a remnant magnetization, which is characteristic of hysteresis loops. The increased extent of remnant magnetization from type I to conventional type II to HTSC may be related to the decreasing coherence length. Attempts to understand the hysteresis in isothermal magnetization began with the macroscopic model of the Bean critical state model (1962). This model was relevant to "hard" superconductors that has thermo-magnetic histories that show a large hysteresis. This Bean model explanation of HTSC brings out many new physical phenomena related to magnetic irreversibilities. Bean theory predicts the absence of spatial uniformity, and that the presence of preferred sites for

vortex "pinning" is necessary for a superconductor to carry large currents in this mixed state. This criterion demands a large critical current density Jc that results in the hysteresis in magnetization.

Magnetic hysteresis has been observed in hard superconductors including both conventional and high-Tc superconductors. In the mixed state, the flux lines can interact with impurities, defects, and inhomogeneities that always exist in hard superconductors. Defects trap flux lines after the field has been turned off; which means the magnetic behavior for type II superconductors exhibits a strong history dependence. This trapped magnetization is called remnant magnetization. Remnant magnetization is a result of the flux pinning of the material and it depends on both the temperature and applied field. Pr-doping will affect the flux pinning strength and the flux density of the materials; it is to what extent that is of interest in this study.

An applied field to the Pr-doped samples overcomes the super currents shielding pinning and enters the samples. When the field is removed, the Pr-doped samples will have trapped more flux lines and so will have greater remnant magnetization. At H_{c2}, the trapped flux reaches a maximum value, and the remnant magnetization is at saturation equilibrium.

B. Time-Decay of Magnetization (Flux Creep)

The presence of the flux creep suggests that the vortices normally pinned against movement by lattice defects are being shaken from the pinning sites by thermal activity. Pinning site energy of a typical radius of ℓ can be calculated by

$$\epsilon = 1/2\pi\pounds^2\mu_0 H_{c2} \text{ (joules per unit length of vortex).} \quad (24)$$

This is the pinning force that must be applied to keep a flux core $\pounds$ away from a pinning center. The difference between the pinning and the Lorentz force is then

$$F_{net} = F_{pinning} - F_{Lorentz\ force} \quad (25)$$

writing this as

$$F_{net} = 1/2\pi\pounds\mu_o H_{c2} - \alpha\delta^2 . \quad (26)$$

δ - is the spacing between pinning centers. As Pr ions are added, the spacing increases and F_{net} will decrease. Now, creep rate may be defined:

$$R = dj/dt = A\exp(-U_{eff}/kT) \quad (27)$$

So when U_{eff} decreases, flux creep rate R decreases likewise. When U_{eff} is greater than the Lorentz force the vortices will be unpinned and will be displaced till the flux is captured by another pinning center. This frequency of jumps v_0 is a function of U_{eff} and of the temperature T.

The basic assumption of the critical-state model is that a superconductor is capable of sustaining virtually no loss of currents up to a critical current density Jc(B), but not beyond[17]. When the magnitude of the current flow throughout the entire specimen is

Jc(B), it is said to be in a "critical state."

For the high-Jc practical metallic superconductors the loss of magnetization (flux creep) may be a few percent for NbTi and Nb_3Sn wires[18]. By contrast, flux creep can result in a 10-35 % or more loss under 0.3-2.0 Tesla at 4.5 K, for $YBA_2C_3O_7$ system.

Thus, there is a problem toward major applications of the bulk high Tc superconductors have been hindered by the flux creep under even moderate applications of magnetic fields. Flux creep occurs in the presence of currents transverse to the magnetic field. The Lorentz force will set the flux filaments into some regions into a continual lateral motion, thereby developing an effective resistance in the material. Thus, in the high-field superconducting materials capable of supporting large transport current densities, some mechanism must be present to provide a rigidity against the Lorentz force, so as to prevent this resistance and thereby reducing flux creep from the material.

Flux creep was noted to be non-exponential in time for HTSC, Muller (1987); they showed logarithmic decay as

$$M(t) = M(o)[1-(kT/U_{eff})\ln(1+t/to)]. \qquad (28)$$

This decay rate M(t) is measured in the remnant state, i.e., after the field has been lowered to zero and where $t_o(\approx 10^{-6}\text{-}10^{-12}$ s) is the characteristic relaxation time of a flux bundle and $t >> t_0$, then

$$U_{eff} = -(kTM(o)/dM/dlnt, \qquad (29)$$

and this is used to extract the activation energy U_{eff}. Magnetization-decay measurements at various temperatures (T) have shown U_{eff} rises with T in HTSC. Hagen and Griessen[19] explained this T dependence by requiring that there is a distribution of U_{eff} in any sample.

The relaxation time t_0 for the studied compound is not known a priori and may change for different forms of a sample[20]. This relaxation time t_0 can be found in the framework of the Anderson model in: First, the equation describing flux penetration into the sample of the slab geometry (the slab thickens is equal to d)[21].

$$\partial B/\partial x = \nabla(vB) \tag{30}$$

differentiating with respect to x across the slab, with

$$v \approx w_m \mu \exp[-U/T]; \tag{31}$$

we get

$$\partial j/\partial t = c w_m/4\pi \partial d/\partial x^2 \{\mu B \exp[-U/T]\}. \tag{32}$$

where w_m is some microscopic (i.e., size dependent) frequency, and μ is the length over which the flux bundle is hopping. A solution for the above equation is of the form

$$j(t,x) = j(t) + \delta_j(t,x) \tag{33}$$

where $\delta j(t,x)$ the variation across the sample is

$$\delta j(t,x) << j(t). \tag{34}$$

Then write

$$\partial j/\partial t = cw_m/4\pi \exp[-U(j)/T]\partial^2/\partial x^2 \cdot [\mu B \exp[-\partial U/\partial j \cdot \delta_j \cdot (x,t)/T]]. \tag{35}$$

Solution for $\delta_j(x,t)$:

$$\delta j(x,t) = -T/(\partial U/\partial j)\cdot(\ln\cdot 1+x^2/d^2)/B(x)/B_{ext}. \tag{36}$$

$$|\delta j(x,t)| \approx [T/U(j)]j(t) << j(t). \tag{37}$$

Then

$$\partial j/\partial t = -2B\cdot ucw_m/\pi d^2 \cdot \exp[-U(j)/T]. \tag{38}$$

Integrate

$$U_\alpha(j(t)) = T\cdot\ln(t/t_0) \tag{39}$$

then

$$t_0^{-1} \approx \mu w_m cB/\pi d^2 T \cdot |\partial U(j)/\partial j|. \tag{40}$$

Where B=value of magnetic induction at the slab boundary. It is apparent here that the relation time t_0 grows with the size of the sample d and with temperature T. This may be seen in this study (see flux creep curves). In the EZPLOT fits, generally for all samples the best fit required an increase in t_0 as temperature increased. Also, t_0

grows with the size of the sample d. The reason: The sample magnetization is proportional to the sample volume, whereas the rate of its time variation is proportional to the sample surface area. If the activation barriers U(j) between different metastable states should grow with current decrease according to:

$$U(j) \approx U_0(jc/j)^{\alpha} \approx |dU(j)/dj|$$

then

$$t_0^{-1} \approx A \cdot c^2 \backslash d^2 \cdot p_{flow} \cdot \alpha U_0 \backslash T; \qquad (41)$$

A = a constant proportional to the volume of flux bundle.

Thus t_0 is αU_0 dependent and a function of the A, volume of flux bundles in a sample. Then as an applied field is increased into a sample, flux density bundles increases; thereby, magnetic hysteresis (M^+-M^-), will decrease as well as Jc since resistance increases because of the increased presence of transverse currents produced by the Lorentz forces on the flux bundles. $t_0 \approx 1/A$, so t_0 will decrease with increased applied field.

C. Magnetization Critical Current

Practical applications of HTSC are contingent upon achieving large critical current flow through bulk superconducting materials. Critical current is a phenomena of the critical state phase established in a superconductor. Bean [1962] proposed a

theoretical model to explain the critical state of a HTSC. Every region in a type II superconductor carries a critical current density Jc, which evolves from the local magnetic field within the region.

Using the isotropic Bean model and the sample dimensions, Jc's can be calculated from:[22]

$$Jc = \Delta M/V \{4/ b(1-b)/3a \qquad \text{for } a \geq b, \qquad (42)$$

$$= \Delta M/V \{4/a(1-a)/3b \qquad \text{for } a \leq b$$

Where Δ M is the magnetization associated with the maximum with of the hysteresis curve, measured in emu/cm^3 and a and b (b>a) are the dimensions of the rectangular cross sections of the sample normal to the applied field, measured in cm. Jc values should then be representative of the average superconducting properties of the specimen.

As stated before, the HTSC must be in a critical state. The melt processed samples of this study have oriented grain structures without any major weak links. This critical state condition was confirmed by a plot of delta M, measured with the sample face perpendicular to the field direction resulting in a straight line for different applied fields[1].

The development of increased Jc in a HTSC is mainly dependent upon the

---

[1]H. Hojaji, S.Hu, A. Barkatt, A.N. Thorpe, and D.D. Davis; Melt-Processed YBCO SC; Processing and Properties; *Unpublished.*

enhancement of flux pinning. Several pinning mechanisms may be used, however, for this study of YBCO materials; Pr doping in trace amounts, distributes Pr^{3+} ions throughout the materials, causing the formation of local defect regions to serve as effective pinning centers.

Besides proper pinning, HTSC's must have an anisotropic crystal structure that results in anisotropic magnetic properties. Thus, innovative processing techniques that optimize flux pinning centers while eliminating defect regions, cracks and aligning the crystal plane will have to be realized for Jc values of commercial use.

D. Effective Activation Energy for Flux Creep U_{eff}

The decay of magnetization over time occurring in Type-II superconductors has been explained by Anderson and Kim [1964] with a thermally activated flux-creep model. This theory says, when a high-Tc superconductor is under the influence of an applied magnetic field, a gradient in the density of flux lines occurs. This gradient causes a driving force balance is reached whenever F to act on the flux-lines, which is as the flux gradient results in a macroscopic current by $\nabla \times B = \mu_o J$. The flux-lines can, however, move into the material only when the local maximum pinning force density F_p is smaller than the driving force density F. At non-zero temperatures flux motion is possible with the help of thermal activation, even if $F < F_p$. Flux motion leads to dissipation that manifests itself as a decay of superconducting currents with time (flux creep) or if an electric current is applied while a sample is in a magnetic field, a flow-resistance develops. The minimum thermal energy required to excite a flux-line

bundle passed a pinning site is called activation energy, U_o. The movement of the flux bundles is in the direction of the flux gradient. The effective potential may be written as

$U_{eff} = U_o - \alpha JB$, then

$$M(t) = M_o[1-(kT/U_{eff})\ln(1+t/\tau)], \qquad (43)$$

For $t >> \tau$, one then obtains

$$U_{eff} = -(kTM_o)/(dM/d\ln t), \qquad (44)$$

and this can be used to extract U_o. This activation energy decreases as the macroscopic current, Jc, increases; as the larger macroscopic current results in a larger driving force on the flux-lines. When the critical current density is reached, the pinning force, F_p, becomes zero, and flux flow occurs; i.e., U_{eff} is defined as the effective activation energy for the flux creep where $J \approx J_c$.

The activation energy U_o, which characterizes the flux creep process, is found to increase slowly with increasing T and take a maximum near Tc, until $T \approx Tc$ where it rapidly decreases to zero. In high Tc superconductors, U_{eff} depends on the structure of the pinning force density. A popular candidate for pinning barriers for melt-textured samples, have been the twin boundaries[23,24] in $YBa_2Cu_3O_7$. Flux decoration experiments[25,26] indicated that the flux lines are preferentially situated at the twin boundaries defects caused by inclusions and isolated weak links. It has been observed

that the individual particles of YPrBaCuO are single grains and the twin boundaries extend across the entire particle. The spacing is also found between the boundaries to be of the range ($\geq 0.2\mu m$)[27]. Thus it is not likely that the twin boundaries are very effective pinning sites. If this is true, the values of U_{eff} measured here may possibly be that for point defects specimen with the addition of the Pr^{+} sites.

This decay of magnetization in high-Tc superconductors is a function of temperature T and magnetic field H and is also substantially influenced by the density and the nature of pinning centers in the sample. As far as Pr ions acting as pinning centers, other studies[28] refute this suggestion. According to ref.[29], only pinning centers with barrier heights greater than $E(T)=KT\cdot\ln(1+t_b/t_b)/(1-T/Tc)$ are effective in trapping flux lines and therefore can be seen in an experiment.

E. Transition Temperature

The absence of superconductivity in the compound $PrBa_2Cu_3O_{7-\delta}$ (oxygen content $\delta \approx 0.05$)[30] is an anomaly in high temperature superconductivity studies. $PrBa_2Cu_3O_{7-\delta}$ is the only nonsuperconducting compound of the series of isostructural compounds $RBa_2Cu_3O_{7-\delta}$ (where R is a rare earth element except Ce, Pm, or Tb; $\delta \approx 0.05$)[31]. The $Y_{1-x}Pr_xBa_2Cu_3O_{7-\delta}$ system is particularly interesting since its superconductivity is suppressed as a function of Pr concentration with the resulting drop in critical temperature Tc. Critical transition temperature, Tc, is the temperature where the specimen changes from a conductor to a superconductor.

The superconducting critical temperature Tc in the $Y_{1-x}Pr_xBa_2Cu_3O_{7-\delta}$ system was

found to decrease monotonically with x and vanish at $x \approx 0.55$[32] (see Fig.2 [33,34]). Other studies find a systematic ion radius dependence of Tc. To illustrate the effect of ionic radius of the rare earth ion on the transition temperatures of $R_{1-x}Pr_xBa_2Cu_3O_{7-\delta}$, a plot of Tc vs. ionic radius of the R ion is given in Fig. 2 taking data for R= Er, Y, and Dy, where Gd and Eu from Ref[35], R=Sm, Tm from [36] and R=Yb from Ref[37]. Ionic radius values are taken from Shannon[38]. The plot clearly shows an increase of Tc with decrease in ionic radius of the R^{3+} ion is observed for each x (Figure 3).

The primary investigation as to the suppression of Tc has been attributed to two possible mechanisms. Since Pr can be in the tetravalent state, the first mechanism involves the filling of mobile holes in the conduction CuO_2 planes due to the substitution of Pr ions with a vacancy greater than +3 and hence infers that the suppression of superconductivity results from a reduced number of carriers in the CuO_2 sheets[6-12]. Magnetic-susceptibility[6,7], Hall-effect[8], thermoelectric-power[9], muon-spin resonance(USR)[10], and neutron-diffraction[11] measurements are consistent with a Pr valence that is considerably larger than +3. Nevertheless, X-ray-absorption near-edge structure[39,40], valence-band resonant photoemission[41], lattice constants and solid solution studies[42,43] suggests a valence close to +3. The total number of holes on O sites was found to be independent of x when electron-energy-loss-spectroscopy measurements[44]. From this, the Pr ions are trivalent and localized, rather than fill mobile holes in the CuO_2 planes; which suppresses superconductivity and leans inevitably to the metal-insulator transition. The phenomena localizing the mobile holes would be associated with the Pr 4f and CuO_2 valence band hybridization.

Figure 2. Transition Temperature vs PR Content.

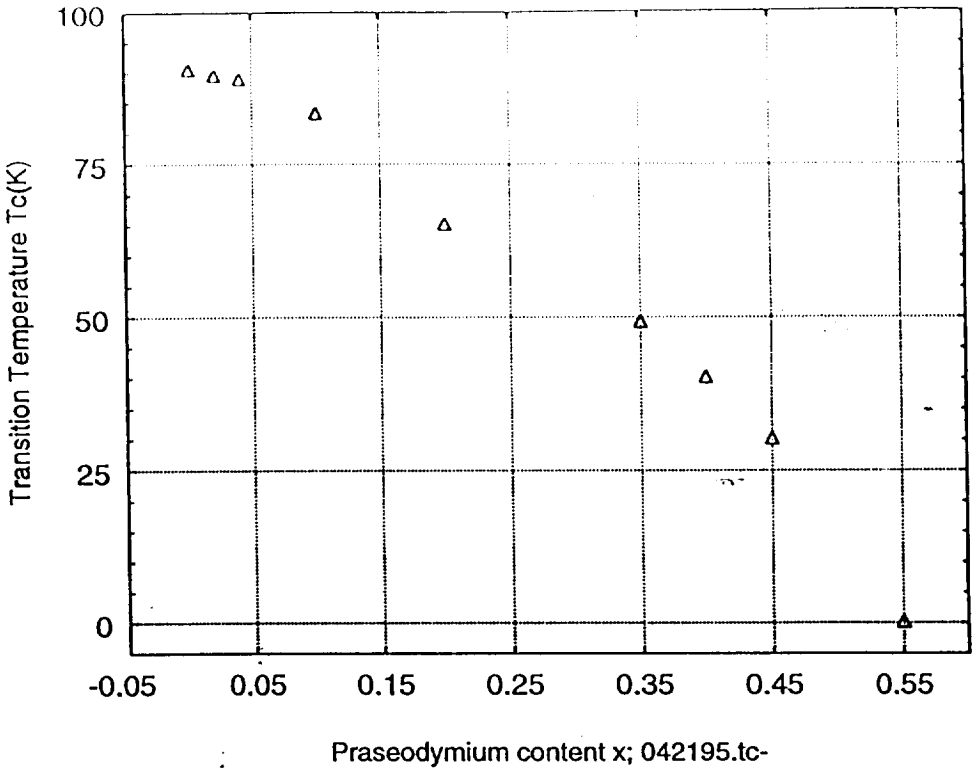

Figure 3. Tc vs Ionic Radius of Rare Earth Ion, $R^{3}+$; 042195.c15

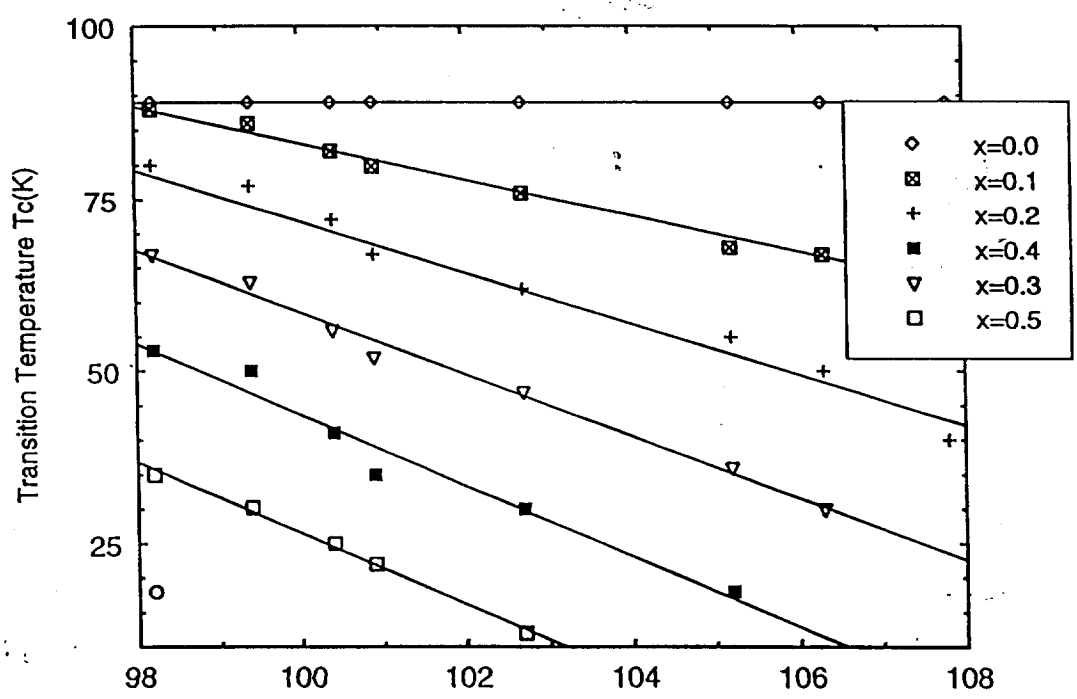

The second mechanism is pair breaking due to spin-dependent exchange scattering of mobile holes in the CuO_2 valence band by Pr ions that have a well-defined magnetic moment. This exchange interaction could occur by hybridization of the localized Pr 4f states and adjacent CuO_2 valence band states, composed of 0 2p orbitals, which then breaks superconducting pairs and causes the depression of Tc. The Abrikosov and Gor'kov (AG) theory[45], predicts a correlation between Tc and x and has been interpreted as evidence for pair breaking[7].

The AG Tc versus x curve can be described by an empirical relation that incorporates the filling of mobile holes in the CuO_2 planes and superconducting electron pair breaking. This relation derived from the best fit of Tc vs. x curve is

$$Tc(x)=Tco - A(\alpha - ßx) - Bx \qquad (45)$$

where AG fitted; results:

$$Tc(x) = 97K - (425K)(0.1 - 0.95x)^2 - (96.5K)x. \qquad (46)$$

and ß is the deviation of the effective valence of praseodymium, v(Pr), from 3[i.e., ß=v(Pr)-3]. So from the best fit: ß=0.95

$$ß = v(Pr) - 3 \qquad (47)$$

$$0.95 = v(Pr) - 3$$

then

$$v(Pr) = 3 + 0.95 = 3.95 \qquad (48)$$

suggesting that the praseodymium ions are nearly tetravalent.

F. Upper Critical Field H_{c2}

The magnetization curve at a given temperature can be evaluated to determine two critical fields of a sample: H_{c1}, the lower critical field at which increasing magnetic fields flux begins to penetrate into the specimen and H_{c2}, the upper critical field at which the sample becomes normal. That is, in the microscopic view at upper critical field H_{c2} in bulk layered superconductors, the electrons propagate freely subject only to scattering off impurities while passing between lattice layers via tunneling. At temperatures below the critical temperature Tc, under an increasing applied field, there is a critical point where the normal cores of the vortices fit between the lattice layers, this is H_{c2}. Bean, Kim and Anderson[46,47] introduced the concept of the critical state, which provides a phenomenological theory of magnetic hysteresis in type-II superconductors in magnetic fields between the onset of flux penetration and the upper bulk critical field H_{c2}. The field between H_{c1} and H_{c2}. The field between H_{c1} and H_{c2} is Hc, the thermodynamic critical field. A strong correlation between the upper critical field and the number of CuO_2 layers in a superconductor has been observed[48]. The temperature dependence of the upper critical field can be investigated after apply a curve fit of the H_{c2}-T data that gives:

$$H_{c2}(T) = H_{c2}(0)[1-(T/Tc)^2] . \qquad (49)$$

Where $H_{c2}(0)$ is the upper critical field at absolute zero.

The qualitative changes of the superconductor properties under the influence of the external magnetic field at H_{c2} can be seen in the curves. Slope changes are informative of the effects on the sample, where the existence in upward curvature near Tc is typical for high-Tc compounds[49]. This $H_{c2}(T)$ dependents according to most studies are the result of the granular structure of ceramic and polycrystalline samples and the presence of intergranular weak links. It is expected that the field affects the charge carrier density. The dielectric layer around the grains and nonuniformity of the sample's composition of the grain surface layers and its distance to the grain boundary creates the space so that magnetic field vortices can penetrate into the polycrystalline samples. Thereby causing structural changes within the samples, just as the increase of Pr ions and its effects are realized also.

In the H_{c2}-T curves, dH_{c2}/dT is obtained. The slopes are believed to be related by a power law to the conduction electron density[50]. The authors assume dH_{c2}/dT is proportional to (n_{ab}), then.

$$dH_{c2}/dT = \beta(n_{ab})^{\alpha}, \qquad (50)$$

where ß is the proportionality coefficient, which is the same for different Pr doping. n_{ab} is the mobile hole concentration (measured with H ‖ c and current in the ab plane). Each crystal of a superconductor has about 1 hole per unit cell[51]. The Pr ion will localize or fill mobile holes. Therefore, the increase in Pr ion concentration in $Y_{1-x}Pr_xBa_2Cu_3O_{7-\delta}$ results in the reduction of the total number of conduction holes[52]. Other studies[53,54,55] shows a linear dependence on Pr as

$$n_{ab} = ax + b. \qquad (51)$$

At $x \approx 0.55$ the system transforms from metallic-like to semiconductor-like behavior. n_{ab} should have a small value at $x \approx 0.55$, where the hole concentration is about 0.16 holes/unit cell[53]. If $n_{ab} = 1$ at $x = 0$ and $n_{ab} \approx 0.16$ at $x = 0.56$ then from Eq.(3), one obtains $n = 1\text{-}1.5x$. When normalizing Eq.(2) with the value of dH_{c2}/dT at $x = 0$, one obtain the normalized upper critical field slope dependence on Pr composition:

$$[\, dH_{c2}/dT \,]_x / [\, d_{c2}/dT \,]_{x=0} = (1 - 1.5x)^{\alpha} \qquad (51)$$

This equation shows that the decrease in n_{ab} is responsible for the dH_{c2}/dT decrease. It's desired from this study that insight whether hole localization or hole filling is the dominant mechanism in this system, by fitting Eq.(4) to the data.
A fit for the H_{c2} - T data gives:

$$H_{c2}(T) = H_{c2}(0)[\, 1\text{-}(T/Tc)^2 \,] \qquad (52)$$

where $H_{c2}(0)$ is the upper critical field at absolute zero.

The $H_{c2}(0)$ values can be used to calculate the coherence length(Γ) from the Ginsburg-Landau relation:

$$\Gamma_{ab2}(0) = \Phi / 2\pi H_{c2}(0) \qquad H \parallel c. \qquad (53)$$

Where Φ is the quantum of magnetic flux.

III. METHODS OF MEASUREMENTS AND EXPERIMENTAL PROCEDURE.

A. Equipment Description

When a sample material is placed in a uniform magnetic field, a dipole moment proportional to the product of the sample susceptibility times the applied field is induced in the sample. If the sample is made to undergo sinusoidal motion as well, as electrical. Signals can be induced in suitably located stationary pick-up coils. This signal, which is at the vibration frequency, is proportional to the magnetic moment, vibration amplitude, and vibration frequency.

This means of producing an electrical signal related to the magnetic properties of a sample material is by using the Model 155 Vibrating Sample Magnetometer. The material under study is contained in a sample holder, which is centered in the region between the pole pieces of a laboratory magnet. A slender vertical sample rod connects the sample holder with a transducer assembly located above the magnet, which, in turn, supports the transducer assembly by means of sturdy, adjustable support rods.

The transducer converts a sinusoidal ac drive signal, provided by an oscillator/amplifier circuit located in the console, into a sinusoidal vertical vibration of the sample rod, and the sample is thus made to "undergo a sinusoidal motion" in a uniform magnetic field. Coils mounted on the pole pieces of the magnet pick up the signal resulting from the sample motion.

This ac signal at the vibration frequency is proportional to the magnitude of the moment induced in the sample. However, it is also proportional to the vibration

amplitude of the signal are subject to errors resulting from variation from variations in the amplitude and frequency of vibration. A nulling technique is used to over come this problem. By appropriately processing these two signals, the effects of vibration amplitude and frequency shifts are canceled and readings are obtained which vary only with moment.

Changes in vibration amplitude and frequency affect both of the signals applied to the differential amplifier, and, because the differential amplifier passes only differences between the two signals, the effects of vibration amplitude and frequency changes are canceled. The result is that one moment determines the amplitude of the signal at the output of the differential amplifier, and this is proportional to the dipole moment of the sample and independent of variations in the vibration amplitude or frequency. This again is proportional to the product of the sample susceptibility times the applied field.

The Model 155 magnetometer, was modified for operations at liquid nitrogen temperature of 77 kelvin. A sample rod has been enclosed in a light metal 3/8 inch diameter tube, which has an opening where helium gas may be introduced around the sample. Surrounding this small tube is a larger case of 3/4 inch diameter tube, with an opening connected to the helium gas tank. Valves are situated so as to allow helium gas to be vented in and shutoff as necessary. A vacuum pump is introduced in these helium lines so the inner and outer helium gas may be removed from surrounding the sample. Helium gas is used to assist and shorten the time to cool the sample to liquid nitrogen temperature of 77 K (Fig. 4).

The rod jackets (inner and outer tube) are inserted into a large heavy glass dewar, located between the magnetic pole pieces. Here liquid nitrogen is filled to cool

the sample jackets to 77 K. This dewar holds about two quarts of liquid nitrogen.

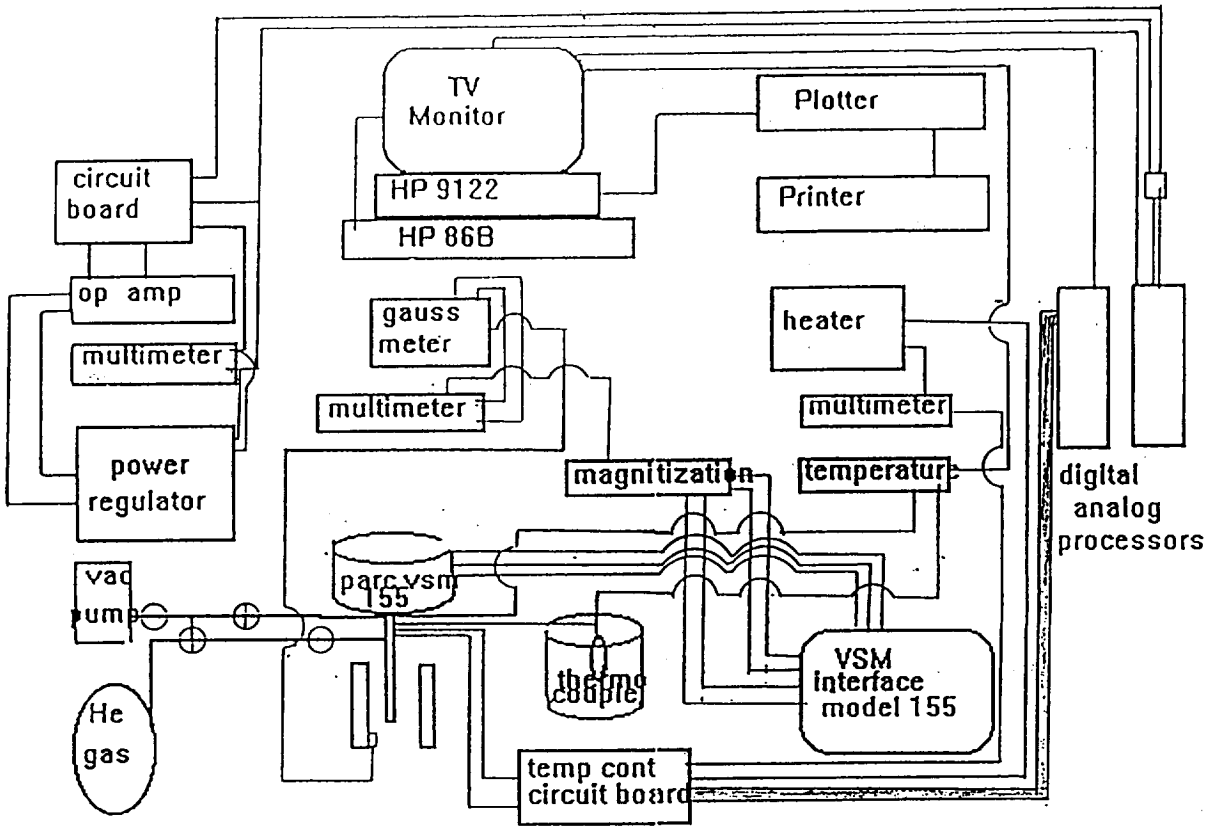

Fig. 4. Block diagram of laboratory.

B. Magnetic Hysteresis

Isothermal hysteresis curves were completed by the sample being zero field cooled to 77 K, at which a 1 Tesla charging field is applied and then removed. Magnetization of decreasing and increasing field was then applied to obtain the hysteresis magnetization cycle. The VSM uses an electromagnet to produce a uniform magnetic field in a gap between a pair of flat parallel pole faces, the field being

perpendicular to the pole faces. Thus, if the field direction is taken as the c axis of a coordinate system with the b axis vertical, unobstructed access to the field region is available along any direction in the a, c plane. The sample is magnetized by a field along the c direction and supported by a rod entering the field region along the b axis from above. Sample is then vibrated sinusoidally along the b axis at a definite frequency (nominally 82 Hz), causing the field due to sample magnetization to vary sinusoidally at 82 Hz as well.

A sample holder assembly supplied with the system provides a simple and convenient means of mounting small solid samples for measurement. The sample is held by placing it in the "sample holder," which is then screwed to the end of the "sample rod." As the sample holder is tightened on the thread the sample rod and the bottom of the sample holder.

Magnetization vs. field was recorded every 60 seconds. The computer graph of the data displayed the remnant magnetization as the area under the curve in units of (kOe emu/g). Hc at the maximum width in emu/g along with dM at 2 kOe was displayed for each hysteresis run.

C. Flux Creep

Magnetic-relaxation (flux creep) measurements on the Pr-doped samples were carried out at different target temperatures using the VSM. The samples were first ZFC, where the critical state was achieved by charging the samples to 10,000 Oe, while removing the applied field after stabilization. Magnetization verse time was measured

at 60 second intervals using the vibrating sample magnetometer. As the relaxation rate became stabilized after the first few data points, logarithmic decay occurs and the data was then fit using the following equation in the EZPLOT program:

$$y = [\, a(1-((8.61708e\text{-}5*T)/b)\ln(1+((x+c)/d))] \quad (54)$$

Where y and a are the magnetization at time t and at time zero, respectively, b is the effective activation energy and d is the relaxation time($\approx 10^{-6}$-10^{-12} seconds). Between each run the sample was warmed to greater than the transition temperature Tc, to ensure that any magnetic flux is rapidly expelled from the sample. For any sample that contains pinning centers, the magnetic flux that penetrated into it may not be expelled at $T < Tc$ since the pinning forces are strong.

The remnants field of the superconducting magnets at the sample position negligible for the relaxation measurements. The above method was chosen to avoid possible technical problems that arise because of the decay of the field from the superconducting coil it. This is because, after the current in a coil is initially installed a field at constant current begins to decay logarithmically, because of flux creep in the windings. The magnetic response of the superconducting sample to a small reduction in field can be strong, from such a small decay of the winding. Also, any drop in the applied field will begin to take the sample out of the critical state and thus dramatically affect its intrinsic relaxation[56].

D. Critical-Current density

Direct measurements of the critical current density Jc on bulk HTSC superconducting samples are difficult to make; so techniques associated with various theories have to be used to evaluate Jc. Because most thin high-Tc sample show large demagnetizing affects when a field is applied parallel to their small dimension. Corrections for demagnetizing effects[57] involving numerical iterative computer programs are difficult to apply.

In this contribution, a simple method is used to obtain Jc(B) from the measured magnetization hysteresis curve. From the Bean model it is assumed that a uniform current density flows throughout the sample. Thus, knowing Jc is isotropic in the plane normal to the field, as are the sample dimensions, allows the use of:

$$Jc(B) = \Delta m/V\,[4/a(1-b/3a)] \quad \text{for } a \geq b, \qquad (55)$$
$$= \Delta m/V\cdot[4/b(1-b/3a)] \quad \text{for } a \leq b.$$

Where delta m = $2(M^{+}-M^{-})$ is the width of the hysteresis curves, at each B. The dependence of Jc on temperature T and composition x, was studied in fields of 0, 2000, 4000, 6000, 8000, and 10,000 Oersteds.

E. Effective activation energy U_{eff}

Magnetic-relaxation (flux creep) in each sample was measured using the VSM

magnetometer. The samples were ZFC to the desired temperature, and then the field was raised to 10,000 Oe. The first measurements were taken about 1 min. after stabilization, after which measurements were made every 60 seconds for 40 min. These measurements were done in field orientations H || c for 77 K, 80 K, 82 K, 84 K, and 86 K. Data were recorded on disks, and transferred to computer programs that displayed the data in graphs.

U_{eff} was obtained from the flux creep curve fits of the EZPLOT computer programs, defined as: For 84 K, sample 2C for example (Remnant magnetization M(t)=y),

$$y = a(1-((8.61708e-84/b)\cdot\ln(1+((x+c)/d))) \qquad (56)$$

a = 5.16303(emu/gram) - initial magnetization of first data point.

b = 0.274934(eV) = U_{eff}

c = 929.414 (seconds) - Offset, the first data point taken.

x = time when first data point is taken(sec.).

d = 1e - 6(seconds) - relaxation time t_0.

of the form

$$M(t) = M_0\cdot[1- KT/Ueff)\cdot\ln(1+t/t_0)]. \qquad (57)$$

U_o was acquired also, by calculation. Again from magnetization M(t) and relaxation rate

$$S = 1/M\ dM/d\ln T \qquad (58)$$

dM/dlnt - obtained from flux creep curves of EZPLOT. The activation energy can be evaluated:

$$U_{eff}/KT = -1/S + \ln(t_b/t_o). \qquad (59)$$

t_o is the time in seconds of the first data point measured. t_o the relaxation time is not known *a priori*, but its only part of a logarithmic term so the error in activation energy is small. Method used is: Obtain M_{tb} from the hysteresis curve for a given temperature, dM/dlnt from EZPLOT curve; obtain S. $x + c = 60$ seconds and $t_o = 1 \times 10^{-6}$ seconds. Then compute

$$U_{eff} = [-1/S + \ln(x+c/d)]\cdot(8.62\times10^{-5}*84). \qquad (60)$$

See figure 5.

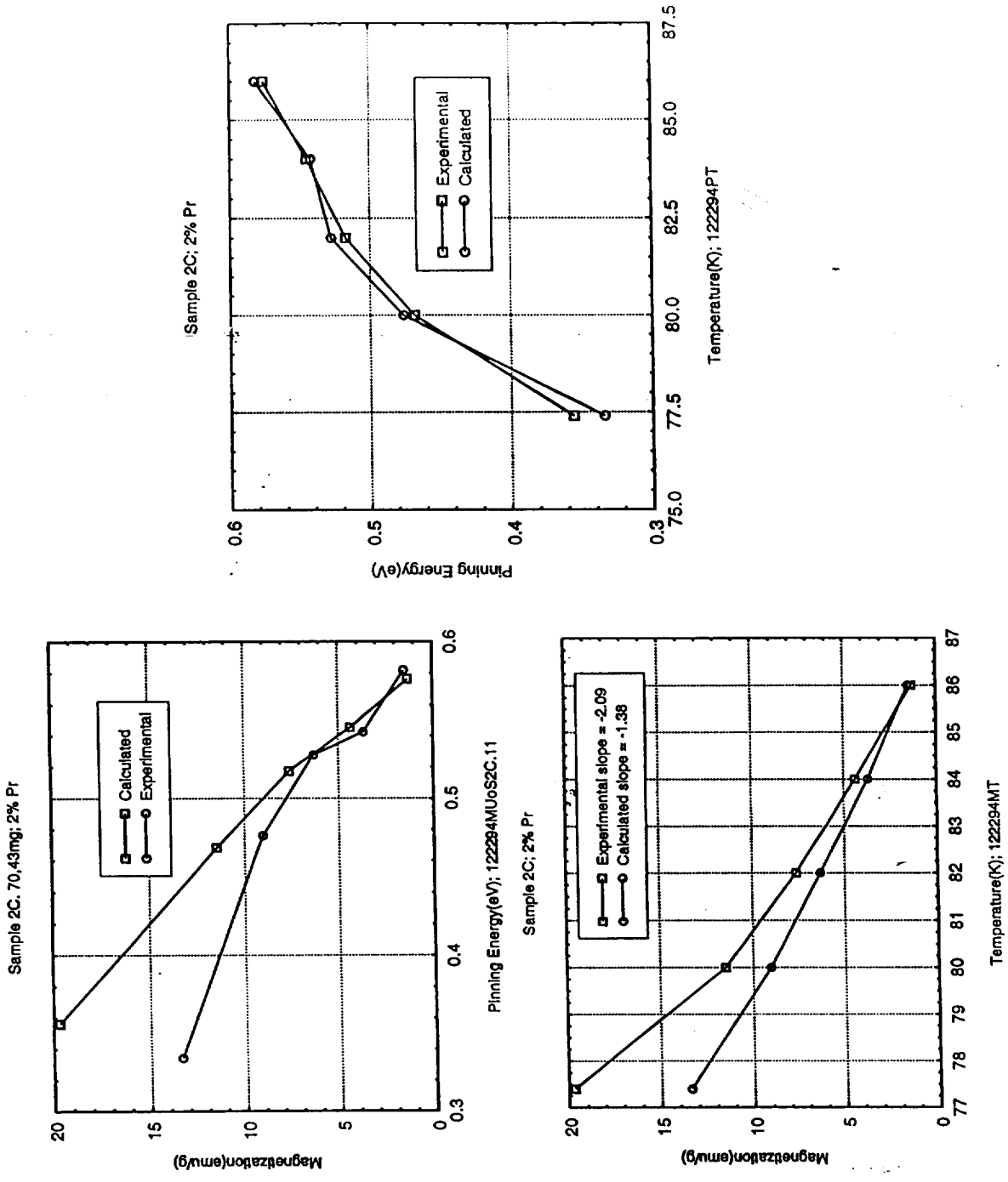

Fig. 5. Experimental and Calculated constants of samples.

F. Transition temperature

After the samples were ZFC, a field of 10,000 Oe was applied. After stabilization the field was taken off, a heater was turned on to warm the sample at a controlled rate, and the magnetization(voltage) as a function of temperature is recorded. Points were taken every 60 seconds. As the sample warmed magnetization voltage decreased. The temperature where the voltage crossed through zero is the transition temperature Tc. This is accomplished analytically by a second order curve fit using EZPLOT to fit the data points.

Plotting the Tc versus praseodymium content x and taking an EZPLOT fit of $y = a-b(c-dx)^p - fx$ to the experimental data; an empirical relation is derived:

$$Tc(x) = 90.16 - 274.14(-0.015+0.77x)^{1.4836} - 28.84x \quad (61)$$

Thus, Tc can be within experimental error of Tc for the range of the data plus the AG data to x = 0.55.

G. Upper critical field H_{c2}

Measurements to obtain H_{c2} for a range of temperature were completed by ZFC the Pr-doped samples, then running a hysteresis curve, applying a field of 10,000 Oe (1 Tesla), decreasing to zero and increasing back to 10,000 Oe. H_{c2} is determined where Δ M vanishes. VSM was used and measurements were done with the applied field

parallel to the c-axis.

Samples were raised above Tc to assure demagnetization is complete between each target temperature run. $H_{c2}(0)$ was used to compute the coherence length from

$$\xi(0) = [\phi_o/2\pi H_{c2}(0)]^{1/2}, \qquad (62)$$

for the zero-temperature value of the coherence length. ϕ_o is a quantum of magnetic flux. Experimentally $H_{c2}(T)$ was obtained by plotting $H_{c2}(T)$ versus Temperature(K), taking the log of $H_{c2}(T)$, plotting $d\ln H_{c2}/dT$ then curve fitting the data to the equation:

$$H_{c2}(T) = H_c(0)\cdot[1 - T/Tc)]^2 . \qquad (63)$$

In EZPLOT language:

$$y = a\,[1 - (\,x/Tc\,)]_2. \qquad (64)$$

Letting Tc value of each sample and x is T. $H_{c2}(0)=y$ may be read from the curve where x = 0 (then y = a). EZPLOT gives value of a. The experimental data H_{c2}-T was then fitted to a straight line, and $[dH_{c2}/dT]_x$ was calculated. With the value of dH_{c2}/dT at x=0, the normalize upper critical field slope dependence on Pr composition was plotted and fitted to equation(50) section F.

$$[dH_{c2}/dT]_x/[dH_{c2}/dT]_{x=0} = (1 - 1.5x\,)^{\alpha}. \qquad (65)$$

IV. SAMPLE PREPARATION[2]

Polycrystalline samples were synthesized by solid-state reaction of appropriate mixtures of high purity Y_2O_3, Pr_6O_{11}, $BaCO_3$ and CuO according to the correct metal stoichiometer composition $(Y_{1-x}Pr_x)Ba_2Cu_3O_{7-\delta}$ in the range $o \leq x \leq 0.1$. Powders were thoroughly mixed, ground, and calcined at 1350-1650°C and leaving them at this temperature range for 10-30 min. in an appropriate crucible, e.g., a crucible made of platinum. The melt is then quenched by pouring it into a copper mold at room temperature. Now the quenched material is reheated to 1120-1250°C, and then, under oxygen pressure varying from 5 to 200 psi, left to stand at this temperature for 3–300 min. This stage is followed by longtime partial melt growth affected by slow cooling(e.g., at 0.5-2°C/hr.) from a temperature of 30-50°C above the cooling to below $\approx$400°C to complete the tetragonal-orthorhombic phase transition. For convenience in shaping, the melt-quenched piece of Y-Ba-Cu-O may be powdered first and then pressed into a desired41 shape before undergoing pressurized partial melt growth. This technique is here denoted as melt-powered-and-pressurized-partial-melt-growth (MPPPMG) processing. In using this process, it was found that with an oxygen pressure higher than 60 psi a piece of Y-Ba-Cu-O with a diameter of 50 mm and a thickness of 30 mm can be subjected to longtime pressurized partial melt-growth upon cooling from 1070°C to below 1000°C at a cooling rate of 1°C/hr without any serious

---

[2] S. Hu, H. Hojaji, A. Batkett, M. Boroomand, M. Hung, and A.C. Buechele, A.N. Thorpe and D.D. Davis; *J. Mater. Res.*, Vol. 7, No.4, Apr. 1992

draining.

This process produces in general samples showing considerable improvement in microstructure and superconducting properties; such as, elimination of serious porosity and inhomogeneity, and also in promoting large-scale grain-texturing in y-Ba-Cu-O materials, and improving the interdomain coupling and overall superconducting properties, as well as the reproducibility in the preparation.

Previous X-ray diffraction studies in Cleveland (by the author of this report) indicated that all samples crystallized in an orthorhombic perovskite-like $YBa_2Cu_3O_{7-\delta}$ structure with extra peaks due to impurity phases.

V. SAMPLE STRUCTURE

This report studies the influence of Pr substitution in $Y_{1-x}Pr_xBa_2Cu_3O_{7-\delta}$. The aim is to compare the Pr effect on the flux creep in the three samples and see whether there is a relaxation dependence on Pr ions present. The x-ray diffraction study for the YPr124 series gave the lattice constants presented in table 1[58], for x=0 and x=0.10. The interpolation for this data for x=0.02, 0.04, 0.06, and 0.08 is included. An increase in a, b, and c with Pr ion concentration is evident.

Table 3

Lattice constants, orthorhombicity and unit cell volume for $Y_{1-x}Pr_xBa_2Cu_3O_8$.

x	a(Å)	b(Å)	c(Å)	2(b-a)/(a+b)(Å^3)	V(Å^3)
0	3.842	3.866	27.225	0.64%	404.38
0.02	3.844	3.866	27.4274	0.63.6%	404.84
0.04	3.846	3.870	27.6298	0.63.2%	405.29
0.06	3.848	3.872	27.8322	0.62.8%	405.75
0.08	3.850	3.874	28.0346	0.62.4%	406.20
0.10	3.852	3.876	28.237	0.62%	406.66

However, orthorhombicity ([2(b-a/(a+b)]), slowly decreases with increasing x. The increase in unit cell volume (V) with x suggests that a doped Pr ion is in trivalent state, as it is only a Pr 3 ion that has an ionic radius bigger than that of Y^{3+}. This results in an orthorhombic phase that increases gradually in unit cell volume (V)

capacity, resulting in a decreasing transition temperature Tc (see Table 1 above).

It is in these orthorhombic layered perovskite-like structure, as with the samples in this thesis, containing CuO_2 planes within which reside the mobile holes that are believed to be involved in the superconductivity. This suggests that some gain in insight of superconductivity is realized by keying on the layered cuprates. In the $Y_{1-x}Pr_xBa_2Cu_3O_{7-\delta}$system the framework is a picture that is based on appreciable hybridization between the praseodymium localized 4f states and the CuO_2 valence band states; a relation first suggested by Neumeir[59] to account for the rapid reduction of Tc and the striking crossover in the pressure dependence of Tc from positive to negative with increasing x in the Y-Pr-Ba-CuO system.

Just as oxygen depletion reduces the CuO_2 plane hole concentration, praseodymium doping does likewise when hole concentration is measured in the superconducting verses the normal states. According to electron energy loss spectroscopy (ELLS) measurements[60] of the O 1s the oxygen sites is independent of x, suggesting that the praseodymium ions localize, rather than fill, holes in the CuO_2 planes. The mechanism by which one hole in the CuO_2 planes per substituted praseodymium ion becomes localized is presumably be associated with the 4f-CuO_2 valence band hybridization[61].

VI. EXPERIMENTAL RESULTS

A. Magnetic Data

The hysteresis data on the samples designated as 1b, 2C, and 3C are given in Figures 6 and 7. Each sample was taken at temperatures 77 K, 80 K, 82 K, and 84 K. The samples were of masses: 1b-74.00 mg, 2C-70.43 mg, and 3C-67.95 mg. They were rectangular in shape and of approximately identical dimensions.

The shape of the hysteresis curves depends on both H_{c2max} and T. As temperature increases the curve widths decreases and its reverse corners begin collapsing. Praseodymium doping made significant differences in the curves, throughout the entire temperature range. With 2 % doping there is a drop in hysteresis width, then an increase with the 4 % doping of Pr; as well as the drop in magnetization and caving in of the curves as the temperature approached the critical-temperature Tc of the specimens.

The pyramid shape is typical of what the Bean model predicts. As the applied field increases and decreases to a maximum, a bulge is maintained in the middle of the curve while the edge gradually flattens as temperature increases. Except for 77 K, the 4 % Pr sample has a bulge smaller than the 0 % Pr sample. This difference increases as temperature increases. The 2 % Pr sample's profile is less than the 0 % Pr sample at all temperatures.

For the applied field $H_a=0$, the slope $\partial H_a/\partial x$, and consequently the current density, near the surface of each sample, are significantly larger than for $H_a>0$. Where

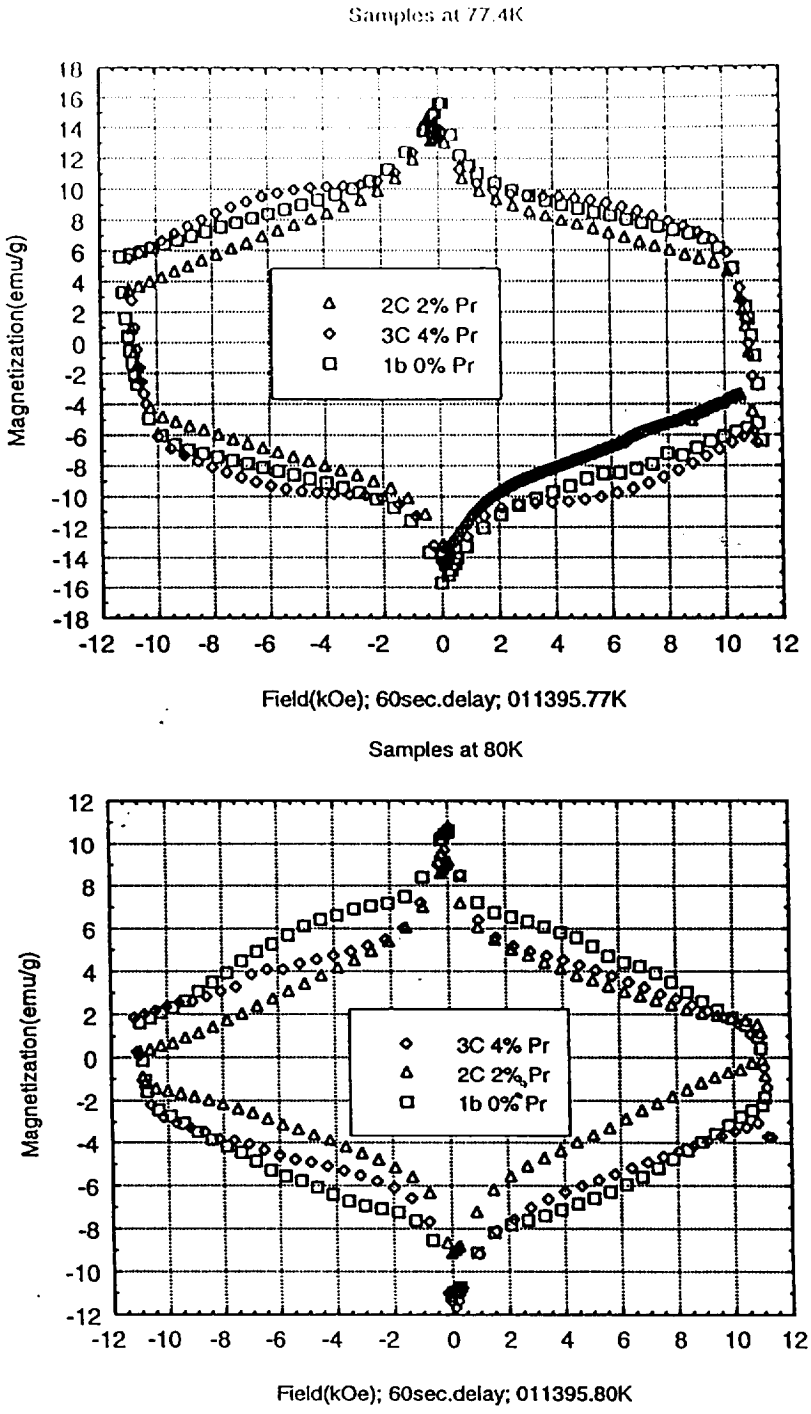

Fig. 6. Hysteresis curves for samples at 77.4 K and 80 K.

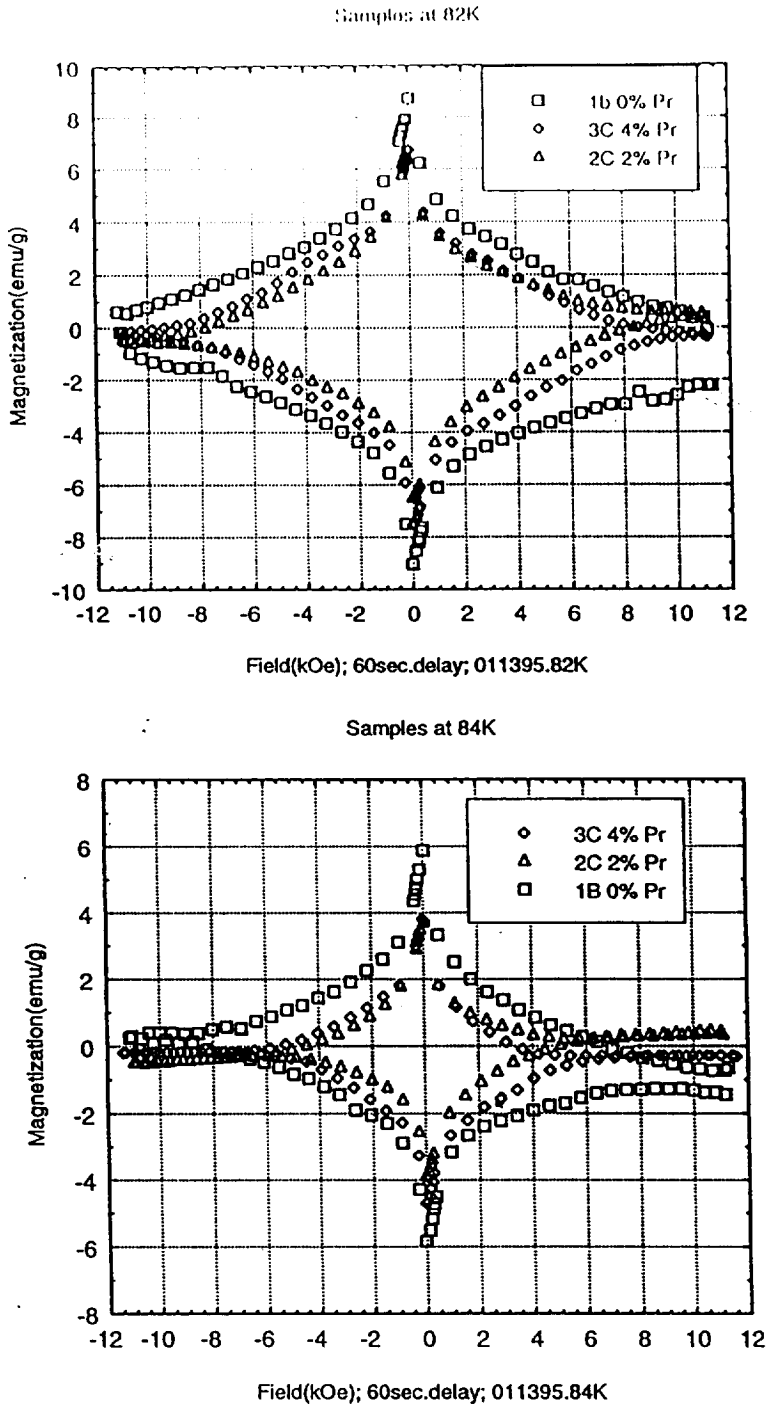

Fig. 7. Hysteresis curves for samples at 82 K and 84 K.

H_a changes directions there is a peak around +250 kOe and -250 kOe for all the temperatures and all the samples than for the 0 % Pr sample. At higher temperatures the 0% Pr sample has more than twice the magnetization than the doped samples at $H_a = 0$.

B. Flux Creep

Flux-creep was measured over the temperature range 77 K, 80 K, 82 K, and 84K For each sample the VSM was raised and stabilized at 10,000 Oe then removed from the sample. With a time delay of 60 sec between each data point, the run was taken for 2000 seconds. Using EasyPlot curve fitting, the data in Figures 8 were fitted to equation (54) by varying both T (temperature), a (initial magnetization), and d (relaxation time).

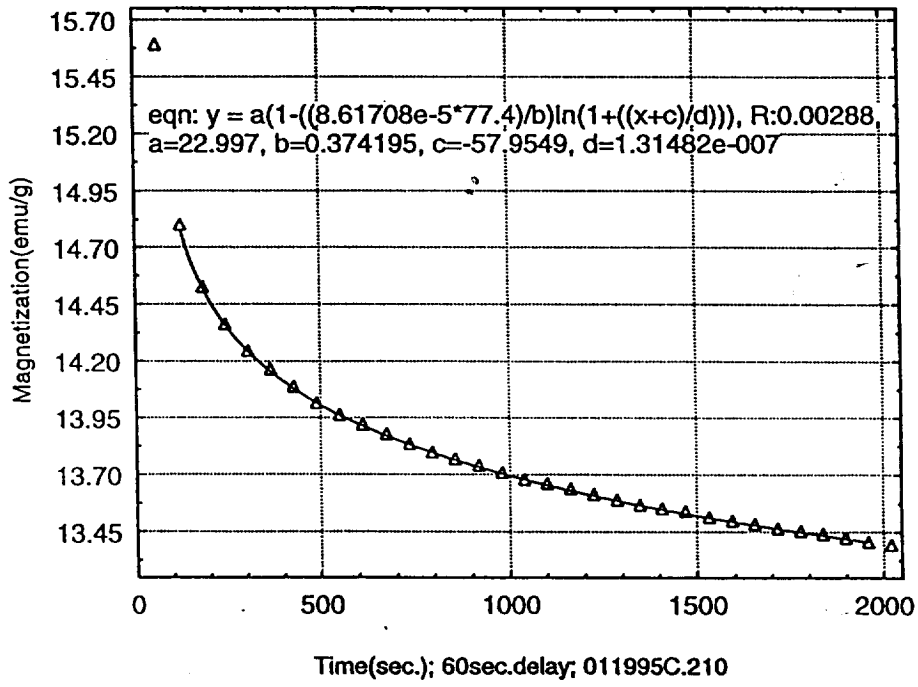

Fig. 8. Flux creep curve and fit for Sample 1b at 77.4 K.

Figures 9 (below) combines all the sample curves for comparison. The values of all the variables of equation (54) giving the best fit are, reproduced in Table 2 for the three samples. Theoretical calculated curves obtained from method described in section III-E are compared with the experimental data for sample 2C as an example in figure 5. The samples displayed a linear dependence of magnetic relaxation upon the logarithm of time except for the initial transient stage. As time and temperature was increased; the samples of 2% Pr, and 4% Pr shows deviation from linearity. Relaxation rate versus temperature, and the normalized relaxation rate versus temperature are plotted in figure 10. The data is consistent with theory.

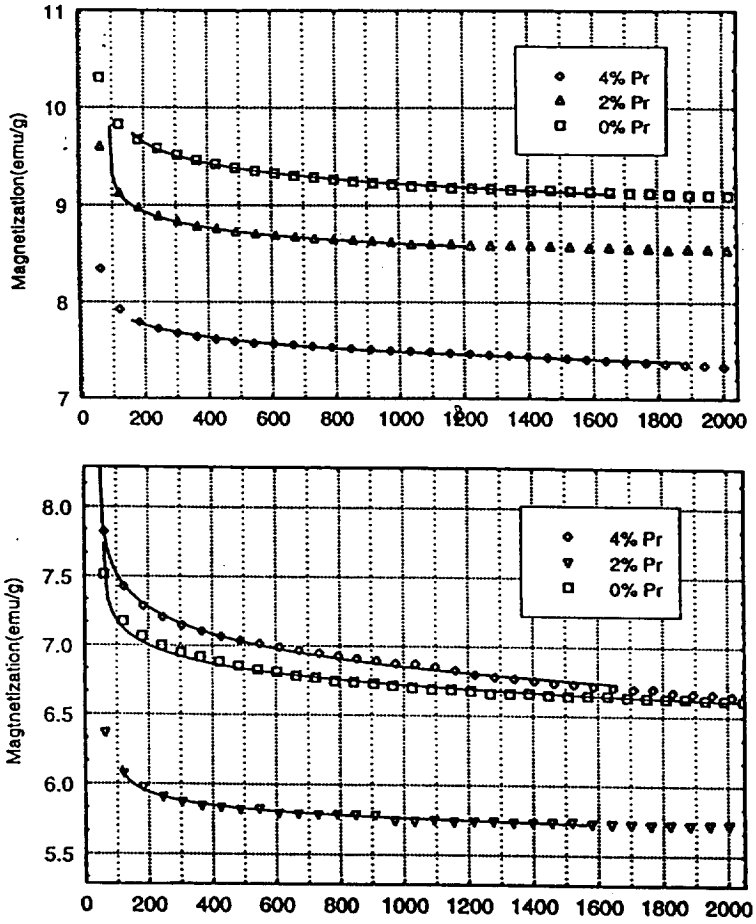

Fig. 9. Flux creep curve and fit; 80 K (top) and 82 K (bottom).

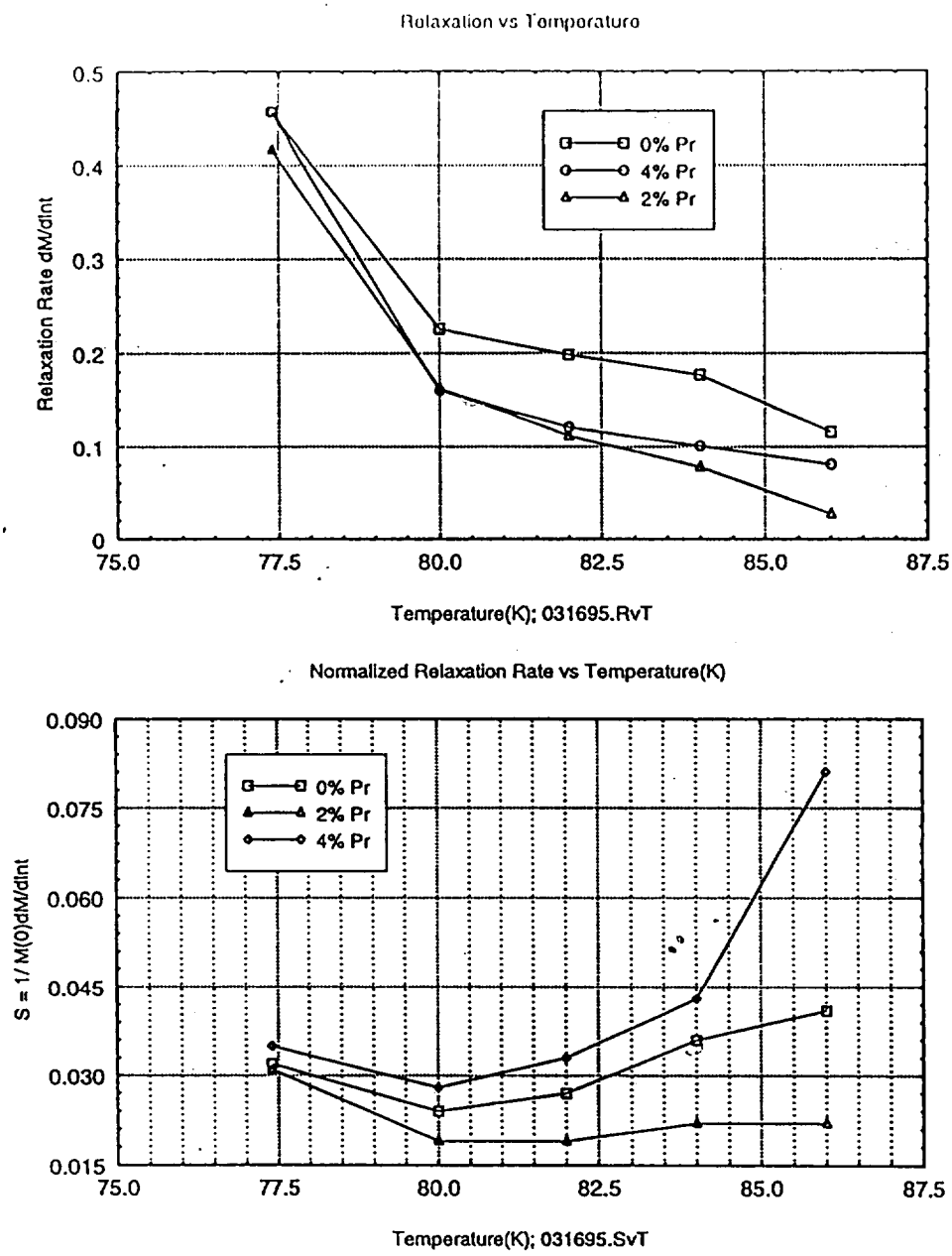

Fig.10. Relaxation rate vs. Temperature and Normalized rate.

C. Critical-current density

Using the isotropic Bean model. Jc was calculated from the Δm, measured from the hysteresis curves with dimensions of:

Sample 1b:	Sample 2C:	Sample 3C:
a=0.34 cm	a=0.34 cm	a=0.35 cm
b=0.48 cm	b=0.44 cm	b=0.37 cm
c=0.09 cm	c=0.11 cm	c=0.10 cm

The dependence of Jc on temperature T and composition χ, was recorded for fields measured from the hysteresis curves. Jc was recorded for 0, 2000, 4000, 6000, 8000, and 10000 Oersted in Figure 11. 77 K are the lower three plots in each figure and 82 K are the upper curves. Praseodymium doping decreased the pinning energy as x increased at 77 K. At 82 K, however, 2C increased over 1b then 3C decreased drastically. Jc versus Field reacted identically as above.

D. Effective Activation Energy U_{eff}

U_{eff} was taken from the curve-fits of the creep curves. U_{eff} increases slowly as temperature increases (Table 2). Pr ion doping decrease U_{eff} as χ increases. Data shows that as U_{eff} becomes large, magnetization falls off linearly Pr doping increases the rate

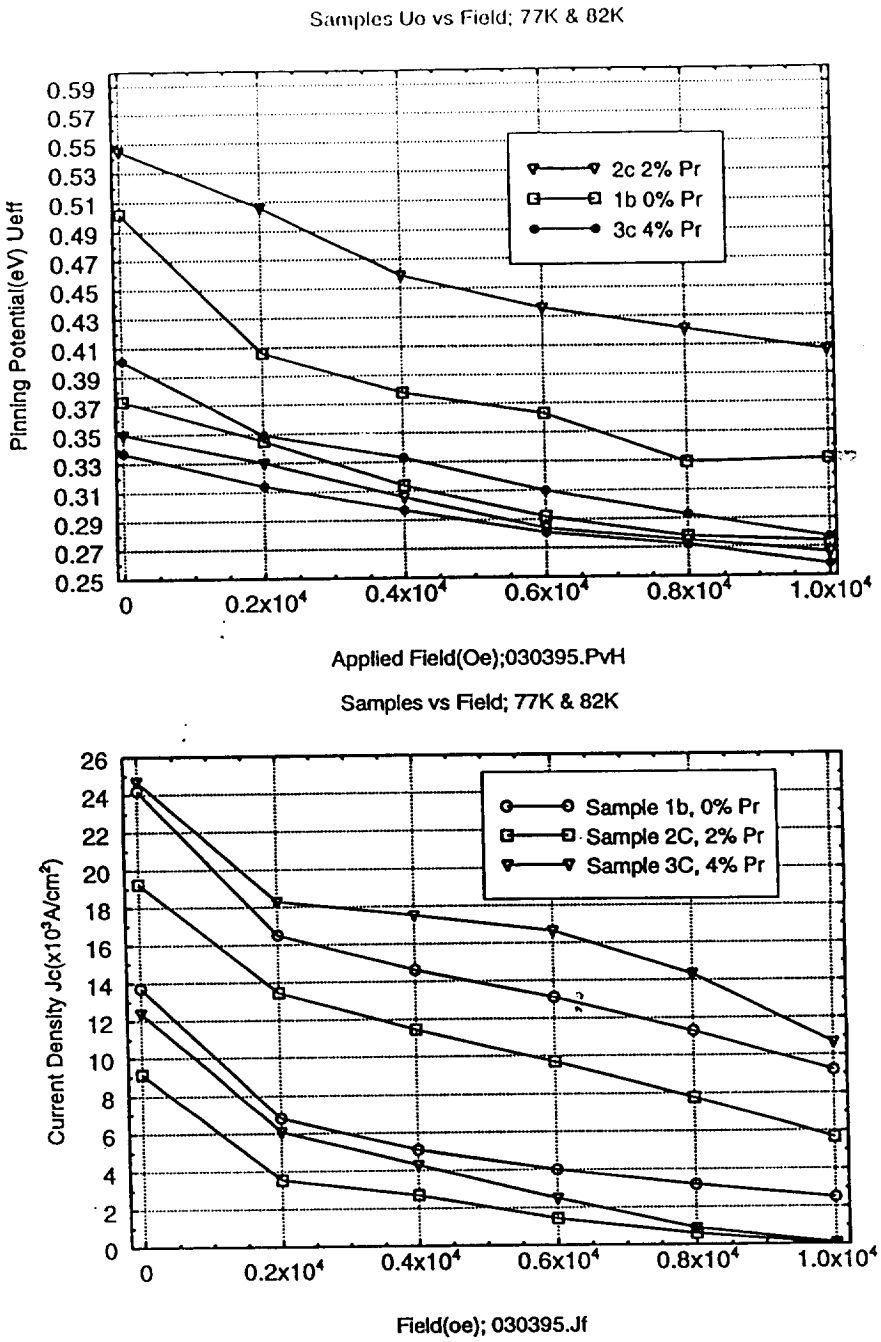

Fig. 11. Current density Jc and Effective potential vs. Field (Oe).

of decay, the flux lines encounter a smaller barrier to motion as U_{eff} decreases. Fig. 11 shows U_{eff} decreases with increasing field, with its effects greater at higher temperatures.

Table 4. Flux creep data constants for Paseodymium samples.

	77.4K	80K	82K	84K	86K
a(emu/g)	23.0	12.8	12.0	7.66	3.10
b(eV)	0.374195	0.504153	0.52930	0.56498	0.604113
c(sec)	-57.95	-138.8	-68.4	-95.41	-61.09
d(sec.)	1.31e-07	1.24e-06	3.8e-12	1.08e-11	1.46e-04
R(error)	0.00288	0.00773	3.7e-07	0.00973	0.0578

Sample 1b 0% Praseodymium Tc = 90.24K

	77.4K	80K	82K	84K	86K
a(emu/g)	17.88	10.87	6.75	4.37	1.68
b(eV)	0.34347	0.49422	0.59607	0.54530	0.51234
c(sec.)	-77.2	-92.6	-103.73	-58.3	-51.7
d(sec.)	1.2e-04	3.1e-04	3.9e-03	3.8e-05	1.1e-06
R(error)	0.0031	0.00759	0.00111	0.0097	0.0103

Sample 2C 2% Praseodymium Tc = 89.26K

	77.4K	80K	82K	84K	86K
a(emu/g)	18.77	9.32	11.63	4.85	2.49
b(eV)	0.314103	0.37960	0.40801	0.41302	0.14513
c(sec.)	-53.12	-1.56	-60.1	-55.50	-174.9
d(sec.)	3.5e-05	1.9e-02	5.29e-08	1.3e-05	1.54e-03
R(error)	0.00912	0.0128	0.00297	0.0355	0.0185

Sample 3C 4% Praseodymium Tc = 88.67K

Deviations from a purely logarithmic time dependence were observed at higher temperatures. This made it necessary to use precaution in curve fitting the data to ensure a correct fit of the logarithmic portion of the data. Initial magnetization a, guessed for the equation(54) was taken from the hysteresis curves. The relaxation time b used ranged from 10^{-6} s to 10^{-12} s. The calculated pinning potentials changed by less than 10%. Increased temperature brought increased U_{eff} until within a few degrees of the sample's Tc where it would abruptly decrease as superconductivity decreased rapidly.

E. Transition Temperature T_c

Results of transition temperature measurements were within ± 0.25 K of most other investigators into T_c for $YBa_2Cu_3O_{7-\delta}$ systems. A fit of the second order was applied to the best fit of the data points, which were taken every 60 seconds. Sample 1b best fit was

$$y = 0.103x^2 - 3.29x + 213, \qquad (66)$$

setting y=0, and using the Pythagorean Theory; Tc is where the curve crosses the x-axis. Thus:

$$Tc = -(-3.29) - [(-3.29)^2 - 4(0.0103)(213)]^{1/2} / 2(0.0103). \qquad (67)$$

$$= 90.26 \text{ K}.$$

For 2 % Pr the fit was

$$y = 0.0115x^2 - 3.48x + 219. \quad (68)$$

So .....Tc = 89.26 K.

Finally for 4 % Pr sample

$$y = 0.0152x^2 - 4.28x + 260, \quad (69)$$

then .....Tc = 88.67 K.

Pr ion doing decreased T_c as expected, with ~1 K drop with 2C, then a half K drop subsequently with 3C. Figure 12 depicts these recordings.

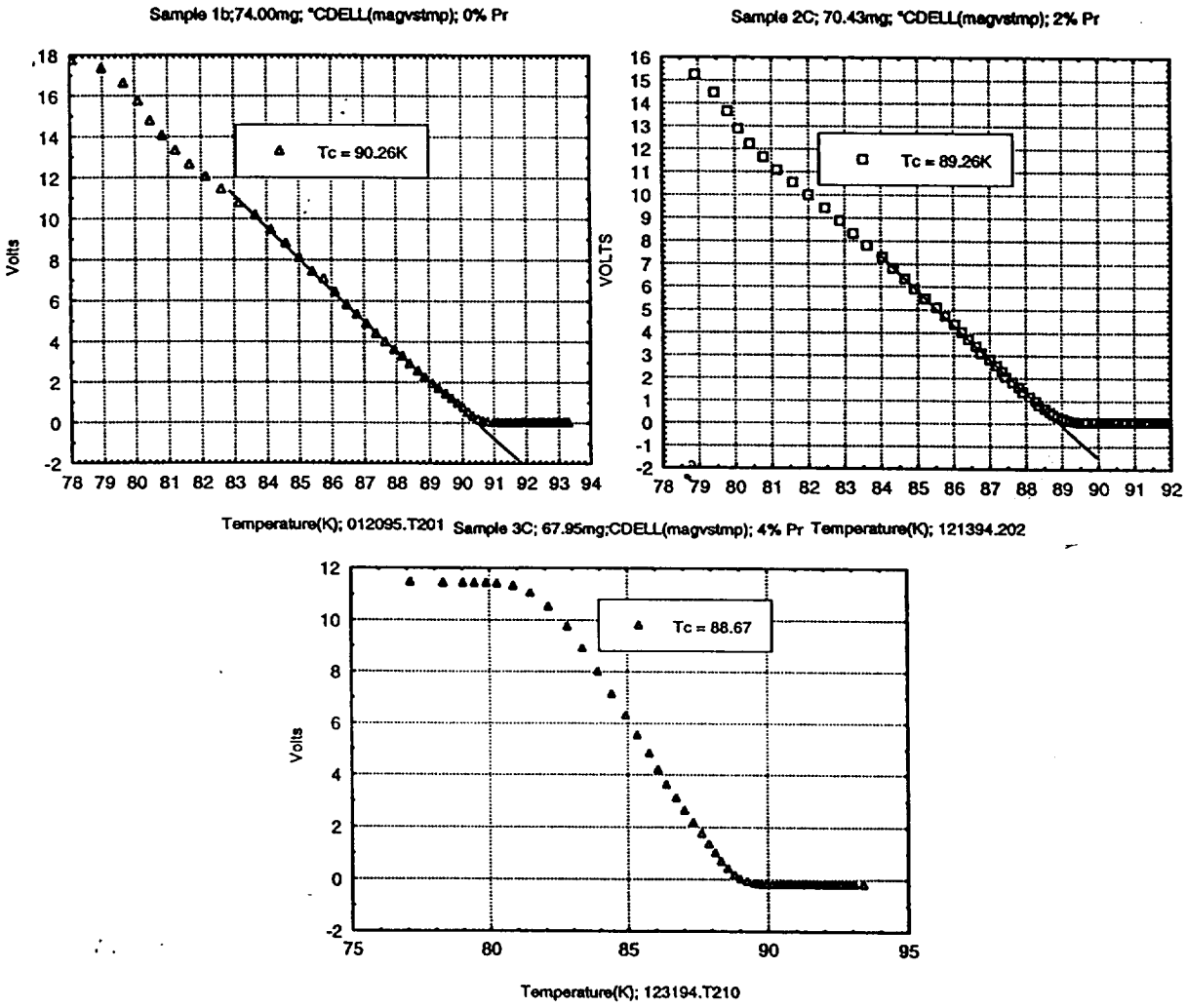

Fig. 12. Transition Temperature Curves.

The three T_c's plus two terminating data points were plotted as a function of x (Figure 13).

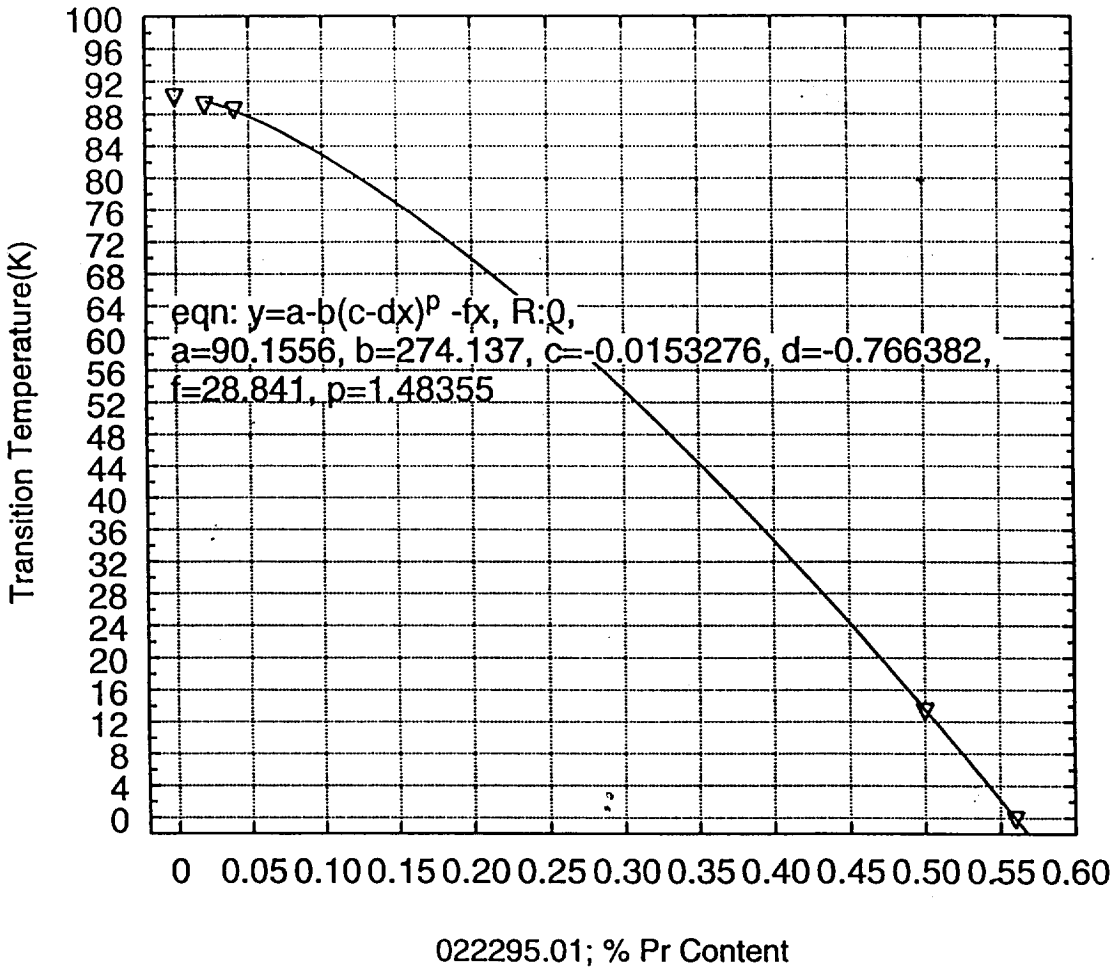

Fig. 13. Transition temperature vs. Pr concentration x.

These data points were curve fitted using equation (56) of section III-E. EasyPlot's best fit resulted in:

$$y = a\text{-}b(c - dx)^{p}\text{-}fx \tag{70}$$

$$= 90.16 - 274.14\,(-0.015 + 0.77\,x)^{1.48} - 28.84\,x$$

Compared to theory where,

$$Tc(x) = 97\ K - (425\ K)(0.1 - 0.95x)^2 - (96.5\ K)x. \qquad (71)$$

Theory gives higher values for Tc for small values of x as compared to experimental. The experimental values of Tc, obtained for Pr concentration x: The Tc suppression rates, dTc/dx(the slopes of the Tc curves):

0 % Pr sample _ -1.48, 2 % Pr sample _ -1.49, and 4 % Pr sample _ -1.65

shows that suppression rates increases with increasing χ.

The pair breaking theory of Abrikosov and Gor'kov[45] for low values of the magnetic impurity with doping of x predicts a linear curve. This does not occur in the data, as the equation for Tc(x) reveals.

F. Upper Critical Field H_{c2}

Hysteresis curves were taken to 10,000 Orsteds and decrease to zero. Where $m \approx 0$ was taken as H_{c2}, for each target temperature (see Figure 7, 84 K). Upper critical field H_{c2} vs T was plotted and the data was fitted to equation (see Fig. 14):

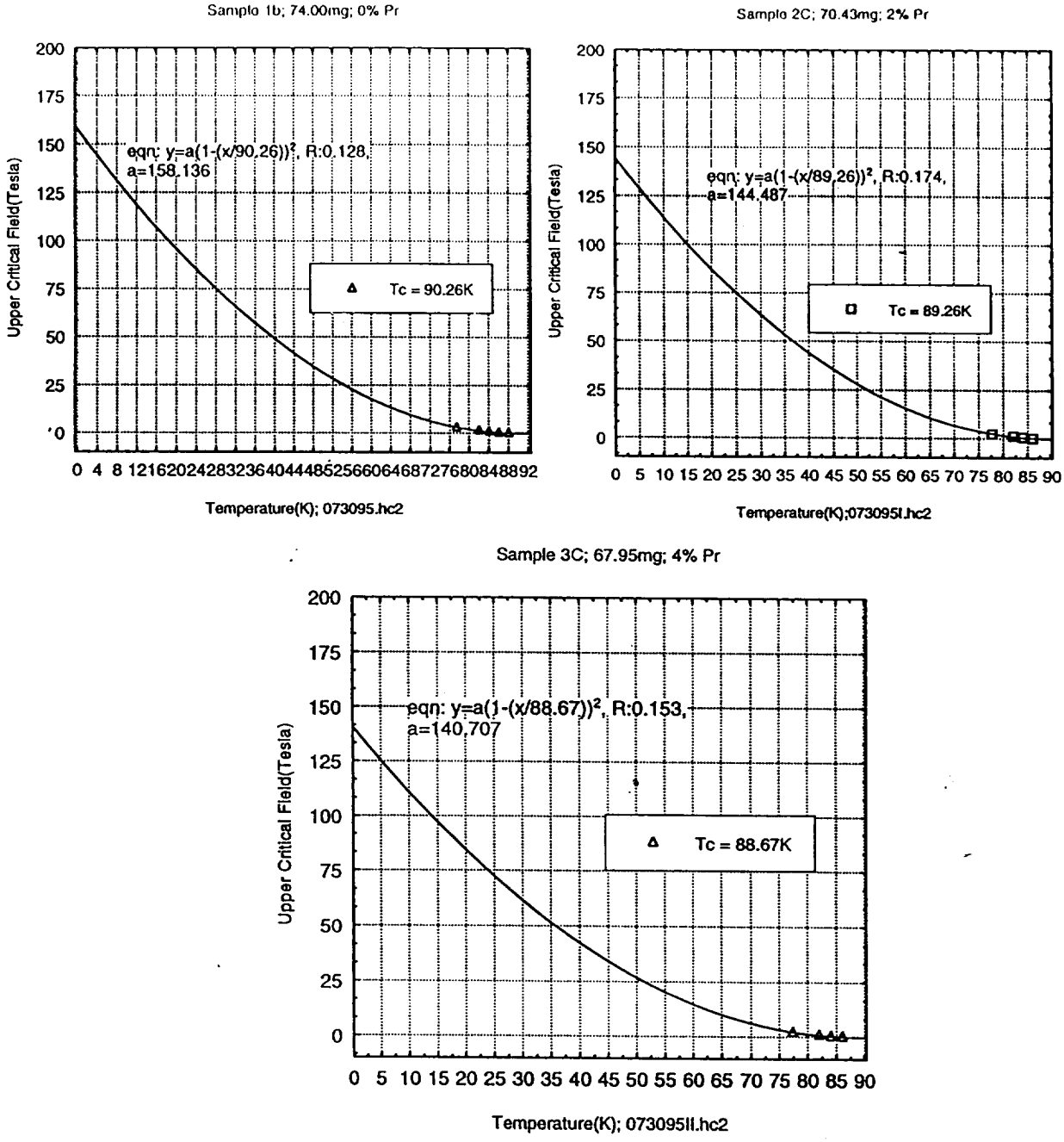

Fig. 14. Upper critical field Hc2 vs. Temperature (K).

$H_{c2}(T) = H_{c2}(0)[1-(T/Tc)^2]$. In EZPLOT $y=a[1-(b/x)^n]$. (72)

Tc = x was set and the variables were determined for the best fit of the data. EZPLOT gives the value of a $H_{c2}(0)$, the upper critical field at absolute zero. Tc is the transition temperature for each sample. Thus, graph shows $H_{c2}(0)$ is for:

Sample 1b -158 Tesla, sample 2C -145 Tesla, and sample 3C-141 Tesla.

$H_{c2}(0)$ was used to compute the coherence length from

$$\xi(0) = [\Theta/2\pi H_{c2}(0)]^{1/2} \qquad (73)$$

where $\Theta=2\pi h/2\pi ce=2.07x10^{-7}G\cdot cm^2$ is the flux quantum, so for sample 1b

$$152.96\ T = 2.07x10^{-7}Gcm^2/2\pi\xi^2(0) \qquad (74)$$

then,

$\xi(0)\approx 0.450$ nm, and 0.453 and 0.455 nm for 2C and 3C

respectively.

These are within the range of studies found by Table 1 of Ref[52]. Short coherence lengths of these ranges will allow only a few Cooper pairs within one coherence volume.

The dependence of normalized dH_{c2}/dT for $H \| c$ on Pr concentration was investigated by fitting equation (51) to the experimental data (Figure 15 top). From the

best fit α is equal to 3.18. This fit about the data points is indicative of hole filling or localization. If ref[52]'s data is added $\alpha = 1.37$ (fig. 15 bottom); and approaches 1.2 as was found by the other studies.

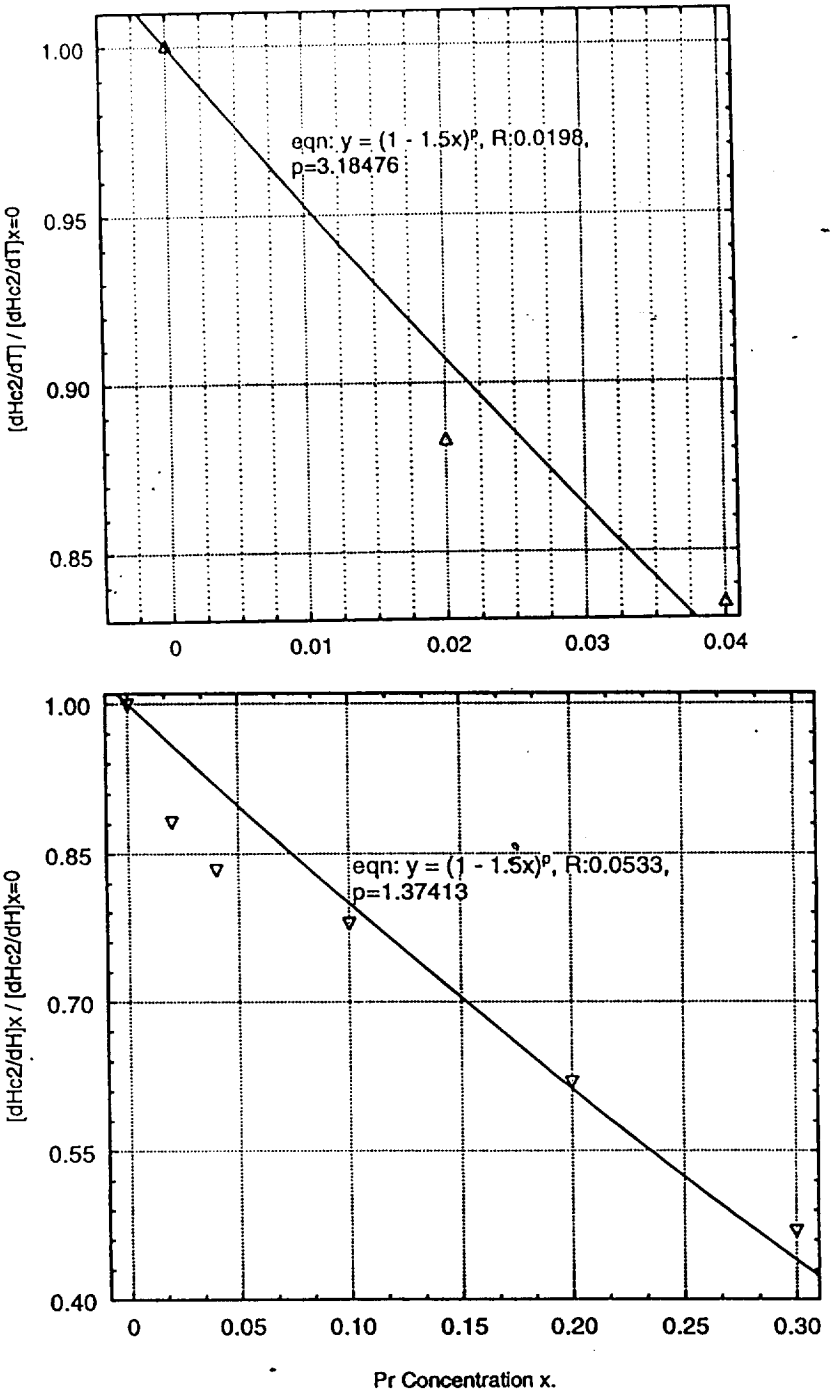

Fig. 15. Normalized dHc2/dT vs. Pr concentration x.

VII. DISCUSSION OF RESULTS

Magnetic hysteresis curves decreases for 2 % Pr doping, then increases oven the 4 % Pr and 0 % Pr sample at 77 K. What's suspected is that initially a portion of Pr ions initially fills the mobile holes in the CuO_2 planes and Ba sites; whereas the 4 % Pr over-doped defect sites, because the lattice distortion does not allow as many Pr ions at Ba sites and CuO_2 planes. This 4 % Pr anomally is an exception, as all other studies of Pr doping shows a decrease as Pr increases.

Pr ions has an immediate effect of decreasing Tc, as will be described later. Thus with increasing x the Tc(x) curve decreases presumably owing to the decrease in the charge carrier concentration, whereas a significant decrease in magnetization is delayed.

The shape of the hysteresis loop depicts the action of the vortices. When the applied field falls through zero, vortices flow out of the sample at the edges, whereas, toward the center the number of vortices stays almost constant. This results in a pyramid-shaped flux-profile, as predicted by the Bean model. However, what is not predicted is in the middle of the sample the flux profile is still rising, because of the flux vortices hopping due to the Lorentz force.

When the applied field is almost zero, the absolute value of the magnetic moment increases and reaches a maximum just after the field passes zero. The hump occurs because the vortices have to move out through the edges of the sample, and thus the flow rate at the edges determines the decrease of the flux in the sample. This rate is proportional to the applied field which is almost zero. This low flow rate prevents

the vortices from leaving the sample rapidly and so there is an enhance absolute value of magnetization. For applied field B=0, the slope $\partial b/\partial x$, and consequently the current density near the surface of the sample, are considerably larger then for $B>0$. As soon as $B<0$, inverted vortices enter the sample , and vortices of different signs annihilate at the intersection of the flux-profile with the B=0 line. Because of this, the number of vortices decreases quickly. These contributions develops the slight hump about the +250 kOe and -250 kOe. This annihilation of vortices slows the creep rate to zero at the peaks; but then the creep rate increases sharply.

The larger flux penetration of the doped sample compared to the undoped samples, while the H_a is increasing, shows that the Pr ions destroys the superconductivity at its weak link sites in addition to the CuO_2 planes. That is, i.e., where the region of the doped samples experiences a local field of magnitude $H_a<H_{c1}$, then no shielding currents flow in the region (complete flux expulsion). The shielding currents will then correspond to a gradient in the vortex density; this cannot occur for a local field $>H_{c1}$.

In summary, magnetization effects of very small doses of Pr agrees with other studies that suggests that praseodymium doping, like oxygen depletion, reduces the CuO_2 planes per substituted Pr ion becomes localized is not readily apparent. However, most researchers suggest the association with the Pr 4f-CuO_2 valence band hybridization[61,62] takes place but is probably not the only reason for loss of superconductivity of a specimen, as it appears in this study; Pr at other sites contributes.

Data showed as with other studies, that there is a linear dependence of magnetic

relaxation with the logarithm of time except for the initial transient stage. This deviation may be explained by the contributions of magnetization with linear relaxation rates of the various grain sizes due to the addition of Pr, i.e., there is more than one relaxation rate displayed by the sample. In the polycrystalline oxide superconductors, the grains are weakly coupled. Such a weak coupling structure suggests that the magnetic flux can easily penetrate the sample through grain boundaries; with the addition of Pr ions magnetization decreased. The orthorhomic distortion is reduced. The relaxation rate is decreased, with the exception of 4 % Pr by the addition of Pr to the samples, again indicating weak link density from the Pr ions as the contributor to flux creep in addition to the bulk samples grain boundaries. Pr interferes with the magnetic ions; whereas, other rare earth elements do not.

In Figure 11, it is observed that substituting magnetic Pr ions into the RE sublattice increases the flux pinning, but decreases the effective pinning potential U_{eff}. Temperature dependence of the pinning potential for every sample starts from some non-zero value, increases with temperature, staying larger than the minimal E(T), until temperature is nearly at Tc, whereupon, activation energy dives toward zero rapidly (Table 2).

As reported in other Y123 studies[63], the decays in magnetization of the samples of this study are as much as 15-39 % of the initially measured values after only 70 minutes (Table 2). Also in comparison with conventional superconductors, not only is the pinning energy lower, but also the operating temperature is higher. Therefore, this large magnetization relaxation is considered due to weak pinning of the flux lines in these materials. In the present study, decay in magnetization is linear with respect

to ln(t) for all compositions studied at low temperatures ($T \leq 80$). As the temperature increases (≥ 80 K), the deviation from the linear in M^+ versus ln(t) becomes significant. Therefore, the logarithmic time decay of magnetization is considered to occur only at temperatures, tentatively below 80 K. Where the plots are non-linear, it indicates an initially partially critical state which corresponds to a partial penetration of the magnetic field in the sample.

The magnetic properties of high Tc cuprate superconductors have been believed to arise from the layered structure i.e. the weakly coupled Cu-O_2 planes, the short coherence length and the weak couple junctions between superconducting regions in high Tc superconductors. Macroscopically these distinctive characteristics are exploited in the effective pinning potential U_{eff} of a specimen, which account for most properties measurable in experiments entailing its magnetic properties.

If U_o is the pinnint potential in the absence of a current (of flux gradient), then the effective pinning energy in the presenc of a current flow and a local magnetic induction then, $U_{eff} = U_o$ - depinning force.

U_{eff} was extracted from the flux creep curves. It increases with temperature until within a few K of Tc, where it's supposed to drop to zero. The experimental data followed the theory closely. The differences in the curves were that $M(0)=a$ is experimentally inaccessible; whereas, for theory M(0) is measured.

Apparently increasing Pr content, has the effect of decreasing U_{eff}. These results concur with studies which revealed that, introducing magnetic Pr ions to the lattice of HTSC does not enhance the flux pinning, but decreases the pinning energy[64]. Of all the R^{3+} ions with partially 4f electron shells that form the orthorhombic $YBa_2CuO_{7-\delta}$

structure; Pr has the largest ionic radius and therefore the greatest overlap between its 4f wave function and the wave functions of the neighboring oxygen and copper atoms.

U_{eff} in light of the above arguments, can be described as

$$U_{eff} = 2l_p / l\epsilon d^{65} \qquad (75)$$

where l is the length of a vortex and l_p is a pinned vortex length. d is the distance between pinning points, and ϵ is the condensation energy in the vortex core region.As Pr ions are added to a system studies of lattice constants confirms that lattice spacing increases with Pr, i.e., d will increase. Thus, as d increase, expect the characteristic pinning barrier U_{eff} to decrease.

The critical field of high temperature superconductors is a means of scrutinizing the coherence length of a specimen. Coherence length is associated with Cooper-pairs, which has a typical distance over which electrons can pair and thus become superconducting. The coherence length is smaller than the applied field penetration depth.

During the increase of the applied field from zero to H_{c2} the energy of the superconductor is raised by an amount

$$E_n - E_s = 1/2u_oH_{c2}^2. \qquad (76)$$

This is equal to the area under the magnetization curve, which is displayed with the plotted curve (see Fig. 6). With H_{c2} known. the energy density of the field, given

by equation (76)(μ_o is the permeability of the vacuum), the difference E_o in energy densities between normal and superconducting states is called the energy gap. To calculate we note that the electron pairing involves electrons in a thin shell of states at the Fermi surface, the density of pairs is one-half the number N_o of particles per unit volume per unit energy inside times the width of the energy shell, given by the gap Δ,

$$\text{pair density} = N_o\Delta/2. \tag{77}$$

In the superconducting state, each of the pairs is lowered in energy by $-\Delta$, so the reduction in energy density is

$$E_o = -N_o\Delta^2/2 = -2R_o\epsilon^2 e^{-2/RoF}. \tag{78}$$

Thus

$$N_o\Delta^2/2 = H_{c22}/2\mu_o \tag{79}$$

where the density per unit energy at the Fermi surface($\epsilon = \epsilon_F$) is

$$N_o = 3\rho/2\epsilon_F. \tag{80}$$

Then we have

$$H_{c2} = \Delta[3\mu_o\rho/2\epsilon_F]^{1/2};\ \Delta_{FROM}/k_B = 1.4 \times 10^5 K. \tag{81}$$

For Sample 2C of this study we get

$$0.85T = \Delta[\ 1.5(4\pi \times 10^{-7}N/A^2)(6 \times 10^{28}m^{-3})/ \quad (82)$$
$$(1.38 \times 10^{-23}J/K)(1.4 \times 10^{5}K)]^{1/2}.$$

Thus the energy gap of Sample 2C is

$$2\Delta = 2(0.85T)/(2.42 \times 10^{2}) \quad (83)$$
$$= 0.702 \times 10^{-2} = 7 \times 10^{-20}J \times eV/1.6 \times 10^{-19}J$$
$$2\Delta = 0.044eV$$

Pr ion doping in the parallel critical field, H_{c2} may increase the normal cores of the vortices in the material, since the Pr ion acts as pinning points, thereby enhancing the penetration of the field throughout the material. For layered compounds, this means more Josephson-Junction behavior can occur. Increased vortices means more scattering and shorter relaxation time; which is consistent with creep studies. Thus Pr doping and increase in H has a similar effect for the samples. The H_{c2} observed effects was indicative that an increasing magnetic field applied to $Y_{1-x}Pr_xBa_2Cu_3O_{7-\delta}$ ceramic surfaces results in the charge carrier depletion and thus destruction of superconductivity at H_{c2}.

Many studies indicate tha as Pr ion content increases, the crystal lattice is deformed and holes from Cu-O chains move toward the sites in CuO_2 planes, thereby lessening superconductivity and lowering of Tc in the region. Thus data showed under

applied fields, H_{c2}(Tesla) is smaller with increase in x (Fig. 11). In detail, a magnetic field penetrates into the bulk sample along the lattice layers, reducing free carrier concentration and separating the superconducting grains along the pores, thereby changing the superconducting properties of the grain boundaries and grain surface. The suppressed superconductivity is suspected to be caused by the pair breaking of the magnetic moment of the Pr ions.

It was clear that the Pr ion is diffinitely more effective in suppressing Tc in the $(R_{1-x}Pr_x)Ba_2Cu_3O_{7-\delta}$ system, because of its larger ionic radius(see Fig. 3) and that the suppression of Tc by very low concentration of Pr demonstrates a more complicated dependence with increasing x than the AG theory; which attributes low concentration fits to its curve as evidence for pair breaking effects by the magnetic Pr ions. Fig. 2 suggests that there is a suppression effect on the superconductivity in addition to pair breaking. The extrapolated value for T(0) using higher x regime ($x>0.1$) of the AG theory resulted in a $Tc \approx 100$ K.

This reveals a mechanism of suppression by Pr that is unaccounted for with AG theory. A hint as to why, may be inferred from the hysteresis curves. In the 2 % Pr doping the curves were smaller than the 0 % Pr. But the 4 % Pr had a larger remanent magnetization. It was suggested than in initial doping most ions combined with the cracks and weak links of the sample. Thus Pr ions were not confined to the CuO_2 planes as theory assumes. So the hybridization between 4f waves of the Pr ion and the conduction band states in CuO_2 planes will be suppressed at these low Pr concentrations, when the exchange interaction is small; thus few Cooper pairs are broken. Tc depression is lacking in other R^{3+} ions because of their smaller exchange

radius of interference and, hence no interference of the 4f electron shells with CuO_2 bound states; thus no destruction of Cooper pairs (superconductivity).

As to the question as to the valence of Pr ions in $Y_{1-x}Pr_xBa_2Cu_3O_{7-\delta}$ system; the Tc(x) (Fig. 13) data curve suggests hole filling and pair breaking is consistent with a Pr close to +4(+3.77) or Pr^{3+}; since for $T(x) \approx T_{co} - [\pi^2/4k_B \cdot N(E_f) \cdot \eta^2 \cdot (g-1)^2 \cdot j(j+1)]$. $\eta^2 \approx 1o^{-4}$eV atoms states/ states/spin direction; which is roughly equal to the coupling constant between conduction electrons[15]. This goes with the suggestion that the Pr ion may hybridize much easier in the +3 state, as its 4f electron will then be loosely bound. In the +4 state, this electron would presumably be located in the CuO_2 planes, the remaining 4f electron is bound more tightly, and would not tend to hybridize. As far as Pr concentration affect on the valence; the linear dependence of the lattice constants and cell volume suggests that Pr valence has a weak if any affect upon the Pr concentration. Other studies suggests the issue can be resolved by inelastic neutron scattering to determine the energy level scheme for Pr in the CEF. However, this experiment produces a broad, low intensity peaks that are difficult to interpret[66,67].

The discovery that the Pr ions are not confined to the CuO_2 planes in this study has theoretical support in work done by Howard A. Blackstead[68], which reveals that the charge fluctuation and the spin-fluctuation explanations are embedded in a theoretical framework that locates the root of superconductivity in the CuO_2 cuprate planes. Blackstead found that Tb^{+4} in $Y_{1-y}Tb_yBa_2Cu_3O_x$, does *not* degrade superconductivity,[69] suggesting that the presence of +4 ions is not sufficient to destroy superconductivity either. Thus charge fluctuations in YPrBaCuO, which are often a source of study, apparently are not a deciding factor for quenching superconductivity.

These other studies suggested that: (i) The superconductivity originates in the chain layers, not in the CuO_2 cuprate planes[70,71,72]. (ii) Some Pr ions occupy Ba sites[11,73], where they break Cooper pairs in the adjacent Cu-O chain layers according to the AG theory for exchange scattering of Fermi-energy carriers by magnetic ions. (iii) The large size of Pr^{+3} is the unique feature which leads to its bonding and higher solubility at a Ba site: the Ba^{+2}ion replaced by the Pr^{+3} is very large (1.42Å vs 1.13Å); and so only the largest rare-earth ions have small enough size mismatches to achieve appreciable solubility at Ba sites[14,74]. The experimental evidence supporting these studies are:

I. Superconductivity origintes in the chain layers (rather than the cuprate planes), because magnetic ions on the rare-earth sites in (rare-earth)$Ba_2Cu_3O_x$ do not destroy superconductivity[75], because they are too distant from the chain layers in which the superconductivity is rooted;[70-73] however, the identical ions on the Ba sites do disrupt superconductivity, since the adjacent layers (which contain the dopant oxygen) are the root of superconductivity, and are close enough in proximity to break-up the Cooper pairs via short-ranged exchange scattering. This Cooper pair-breaking in $Y_{1-x}Pr_xBa_2Cu_3O_{x-\delta}$ has been associated with the local moments of Pr ions.[1,7,15] Since no other (rare-earth)$^{+3}$ ion on the rare-earth site destroys superconductivity, the Pr ion cannot be assigned to J=4 Pr^{+3} on the rare-earth site. J=5/2 Pr^{+4} (Refs. 12 and 76) requires interaction too complex to be appropriate. Thus, if the Pr moments are responsible for destroying the superconductivity, while the rare-earth site Pr ions are not, then the Pr must occupy another site when it breaks Cooper pairs, and that site must be near the origin of superconductivity. Only the Ba cation site is large enough to accommodate Pr^{+3}, thus the chain-O must be the source of superconductivity.[68]

II. Physical proof that Pr is present on some Ba sites are evidenced from the sample preparation and x-ray data[77,78] meaning, that in $PrBa_2Cu_3O_x$, the material is actually $PrBa_{2-x}Pr_xCu_3O_x$, with x being significant[67,72]. Neutron scattering data are insensitive to the difference between Ba and Pr,[79] however what can be observed is the occupancy of the antichain or O(5) site by oxygen (7 %),[11] which is a signature of an ion on the adjacent Ba site in the +3 valence state. In this thesis even minute doping results in an immediate decrease in Tc (superconductivity), thereby suggesting an attraction to the Ba sites and not just periphery filling. The Tc curves vs Pr falls off gradually, another indication of a steady rate of Ba site occupation by Pr ions.

III. The large sizes of Ce^{+3} and Pr^{+3} make them unique, in that it allows them to occupy Ba sites without too much lattice distortion. Smaller ions would have difficulty occupying a Ba site in the (rare-earth)$Ba_2Cu_3O_x$ structure, being too small to efficiently bond to the sites's neighbors.[80]

In conclusion, this study finds that the underlying reason for suppression of the superconductivity in YPrBaCuO systems as Pr increases is the magnetic moment of a Pr ion on a Ba site breaks Cooper pairs as lattice distances are increased thus interfering with the Cooper pairs of comparably similar coherence lengths to the lattice separations and thereby destroying the pairing correlations essential to superconductivity. Once these correlations are broken, Coulomb interactions[81] becomes dominant and drive the materials toward the insulating state. These low coherence lengths of the high-Tc superconductivity in general give them a propensity to defect region formations, which Pr ions and grain boundaries provide.

These increase defect regions, called weak-link formations, simulate the thermal

agitation and lattice distortion destroys the attraction between Cooper pairs. As Pr ions are increased on Ba sites, electron condensation is destroyed. The electron pairs are described by a common quantum mechanical wave function, and there is a long range order among all of the electron pairs, allowing pairs to flow through the lattice structure without collisions leading to resistance in normal conductors. As Pr on Ba sites is added the wave functions are degraded; thus superconductivity is destroyed.

IIX. REFERENCES

1. S.K. Malik, C.V. Tomy and Parag Bhargava, *Phys. Rev. B. 44* (1991) 7042.
2. Y. Xu and W. Guam, *Solid State Commun. 80*(1991) 105.
3. Y. Xu and W. Guam, *Appl. Phys. Lett. 59* (1991) 2183.
4. L. Soderholm, K. Zhang, D.G. Hinks, M.A. Beno, J.D. Jorgensen, C.U. Segre, and I.K. Schuller, *Nature 328,* (1987) 604.
5. J.K. Liang, X.T. Xu, S.S. Xie, G.H. Rao, X.Y. Shao, and Z.G. Duan, *Phys. B69,* (1987) 137.
6. Y. Dalichaouch, M.S. Torikachvili, E.A. Early, B.W. Lee, C.K. Seaman, K.N. Yang. H. Zhou, and M.B. Maple, *Solid State Commun. 65*, (1988) 1001; and reference therein.
7. C.S. Jee, A. Kebede, D. Nichols, J.E. Crow, T. Mihalism, G.H. Myers, I. Perez, R.E. Saloman, and P. Dchlottman, *Solid State Commun. 69*, (1989) 379.
8. A. Matsuda, K. Kineshita, T. Ishii, H. Shibata, T. Watanabe, and T. Yamada, *Phys. Rev. B 39*, (1988) 2910.
9. A.P. Goncalves, I.C. Santos, E.B. Lopes, R.T. Henriques, H. Almeida, and M.O. Fiqueiredo, *Phys., Rev. B 37*, (1988) 7476.
10. C.K. Seaman, J.J. Neumeir, M.B. Maple, L.P. Le, G.M. Luke, B.G. Sternlieb, Y.J. Vemura, J.H. Brewer, R. Kadono, R.F. Kiefl, S.R. Krietzman, and T.M. Riseman, *Phys. Rev. B 42*, (1990) 680.
11. J.J. Neumeier, M.B. Maple, *Physica C, 66*, (1990) 191
12. J.J. Neumeier, T. Bjornholm, M. B. Maple, and I.K. Schuller, *Phys. Rev. Lett. 63*, (1989) 2516.
13. J.J. Neumeier., M.B. Maple, and M.S. Torikachivili, *Bull. Am. Phys. Soc. 33*, (1988)689; *Physica C* (1988) 156.
14. A. Kebede, C.S. Jee, J. Schwegler, J.E. Crow, T. Mihalism, G.H. Myers, R.E. Saloman, P. Schottman, M.V. Kuric, S.H. Bloom, and R.P. Guertin, *Phys. Rev. B 40*, (1989) 4453, and references therein.

15. J.L. Peng, P. Klavins, R.N Shelton, H.B. Radousky, P.A. Hahn, and L. Bernandez, *Phys. Rev. B 40,* (1989) 4517.

16. M.A. Maple, J.M. Ferreira, R.R. Hake, B.W. Lee, J.J. Neumeier, C.K. Seaman, K.A. Yang, and H. Zhou, J. *Less Commom. Metals* 149, (1989) 405

17. C.P. Bean,, *Phys. Rev. Lett. 8,* (1962) 250.

18. A.K. Ghosh, Youwen Xu, and M. Suenaga (unpublished).

19. C.W. Hagen and R. Griessen, *Phys. Rev. Lett. 62,* (1989) 2857

20. D. Hu, W. Paul and J. Rhyner, *Physica C 200* (1992) 359.

21. M. V. Feigelman and V.B. GeshKenbein, V.M. Vinokur, *Physical Review B, Vol. 43, #7;* 1 March 1991.

22. H.P. Wiesinger, F.W. Sauerzopf and H.W. Weber, *Physica C.* 203(1992) 121-128.

23. P.H. Ress, *Physica C 153-155,* (1988) 1121.

24. T. Matsushita, K. Fumaki, M. Takeo, and K. Yamafuji, *Jpn. J. Appl. Phys. 26,* (1987) L1524.

25. L. Ya. Vinnikov, L.A. Girevich, G.A Emel'chenko, and Yu. A. Osip'yan, *Pisma Zh. Eksp. Teor. Fiz. 47,* (1988)109 *JETP Lett. 47,* (1988) 131.

26. G.J. Dolan, G.V. Chandrashelhar, T.R. Dingo, C. Field, and F. Holtzberg, *Phys. Rev. Lett. 62,* (1989) 827.

27. Youwen Xu, M. Suenaga, J. Tafto, R.L. Sabatini, A.R. Moodenbaugh, and P. Zolliker, *Phys. Rev. B 39,* (1989) 667.

28. M. Balanda, A. Bajoerk, A. Szytula and Z. Tomkowicz; *Physica C 205*(1993) 280-288.

29. C.W. Hagen and R. Griessen, *Phys. Rev. Lett. 62*(1989) 2857.

30. Institute of Nuclear Physics, Kadzokowskiego 152,31-342 Craxow, Poland.

31. Y. Yeshuram and A. P. Malozenoff, *Phys. Rev. Lett.* (1988) 60.

32. L. Soderhalm, K. Zhang, D.G. Hiwks, M.A. Beno, J.D. Jorgensoen, C.U. Segre, and IK. Schuller, *Nature 328*(1987) 604.

33. J.L. Peny, P. Klavins, and R.N. Shelton *Physical Review B., Vol. 40, #7* 1 Sept 89.

34. J.K. Liang, X.T. Xu, S.S. Xie, Gott, Rao, X.Y. Shao and Z.G. Dian, *J. Phys. B* 69(1987) 137.

35. Y.Xu and W. Guan, *Physica C 183*(1991) 105.

36. S.K. Malik, C.V. Tomy and Prag Bhargara, *Phys. Rev. B* (19910) 44.

37. M.S. Hegde, X.Q. Xu, J.L. Peng, H.Zhang, R.L. Greene, S.M. Green, *Physica C 229*(1994) 239-243.

38. R.D. Shannon, *Acta Crystallogr. A32*(1976) 751.

39. Y. Tokura et al. *Phys. Rev. B38,* (1988) 7156.

40. M.W. Shafer et. al., *Phys. Rev. B 39,* 2914(1989); D.D. Sarma et al., *Solid State Commun. 77,* (1991) 377.

41. J.S. Kang et al., *J Less-Common Met. 148,* (1989)121.

42. N. Ikeda, K. Kohn, E.V. SampathKumaran, and R. Vijayaraghavan, *Solid State Commun. 68,* (1988) 51.

43. A. Suziki, E.V. Sampath Kumaran, K. Kohn, Ti Shibuya, A. Tohdake, and M. Ishikawa, *Japn. J. Appl. Phys. 27,* (1988) L792.

44. J. Fink et al., *Phys. Rev B42,* (1990) 4823.

45. A.A. Abrikosov and L.P. Gorkov, Zh. EKs., *theor. FIz. 39*(1960) 1981; *Sov. Phys. JETP* 12(1961) 1243.

46. Y.B. Kim, C.F. Hempstead, and A.R. Strnad, *Phys. Rev. Letters 9,*(1962) 306.

47. P.W. Anderson, Phys. Rev. Letters 9, 309(1962); *Rev. Mod. Phys. 36,* (1964) 39

48. H. Mukaida. K. Kawaguichi, M. Nadao, H. Kumkura, D.R. Dietderich, and K. Togano, *Phys. Rev. B42,* 2659.

49 I.M. Dmitrenko, A.M. Glukhov, S. Zaika...*Fiz. nizkikh Temp. 14,* (1988) 1045.

50 T.P. Orlando, E.J. McNiff, J.S. Foner, and M.R. Beasley, *Phys. Rev. B 19,* (1979) 4545.

51. N.P. Ong, in Properties of High Temperature Superconductors 11, edited by D.M. Ginsberg (*World Scientific,* Singapore, 1989).

52. Y.X. Jia, J.Z. Liu, M.D. Lan, P. Klavins, R.N. Shelton, and H.B. Radousky,

Physical Rev. B, vol. 45, Number 18(May 1992).

53. A. Matsuda, K. Kineshita, T. Ishii, H. Shibata, T. Watanbe, and T. Yamada, *Phys. Rev. B 38*, (1988) 2910.
54. K. Nahm, B.Y. Cha, and C.K. Kim, *Solid State Commun.*
55. R.F. Wood, *Phys. Rev. Lett. 66*, (1991) 829.
56. M.R. Beasley, R. Labusch, and W.W. Webb, *Phys. Rev. 181*, (1969) 682.
57. F.M. Sauerzopf, H.P. Wiesinger and H.W. Weber, *Cryogenics 30* (1990) 650.
58. K. Kayama, S. Taga and S. Noguchi, *Physica C 185-189*(1991) 771.
59. J.J. Neumeier, M.B. Maple, and Torikachivilli, *Physica C*, 156(1988) 574.
60. J. Fink, N. Nucker, H. Romberg, M. Alexander, M.B. Maple, J.J. Neumeier, and J.W. Allen, *Phys. Rev. B, 42*(1990) 4823.
61. C.R. Fincher, Jr., and G.B. Blanchet, *Phys. Rev. Lett.*, 67(1991) 2902.
62. M.B. Maple, N.Y. Ayoub, J.Beille, T. Bjornholm, V. Dalichaouch, E.A. Early, S. Ghamaty.
63. Y.Yeshurum and A.P. Malozemoff *Phys, Rev. Lett. 62*(1989) 2857.
64. M. Balanda, A. Bajorek, A. Szytula and Z. Tomkowicz, *Phsica C 191*(1992) 515.
65. T.L. Hylton and M.R. Beasely, *Phys. Rev. 41*(1990) 11669.
66. U. Walter E. Holland-Moritz, A. Severing, A. Erle, H. Schmidt and E. Zirngiebl, *Physica C 153-155*(1988) 170.
67. L. Soderholm, C-16 Loong, G.L. Goodman, U.Welp, J. Bolender and C.W. WIlliams *Physica B 163* (1990) 655.Superconductors 11, edited by D.M. Ginsberg(*World Scientific*, Singapore, 1989).
68. Howard A. Blackstead, J.D. Dow, *Physical Rew. B, vol. 51 17*(1995) 11830.
69. G. Cao, R. J. Kennedy, J> W. O'Reilly, J. E. Crow, P. Pernambuco-Wise, and S. T. Ting, *Physica B 186-188*, (1993) 1022.
70. H. A. Blackstead and J. D. Dow, *Pis'ma Zh. Eksp. Teor. Fiz. 59, 262* (1994)
71. H. A. Blackstead and J. D. Dow (unpublished). This work on oxide superconductivity achieves superconductivity by Cooper-pairing holes through the polarization field.

72. H. A. Blackstead, J. D. Dow, W. E. Packard, and D. B. Pulling, Physica C 235-240, (1994) 1363

73. H. A. Blackstead and J. D. Dow, in *Proceeding of the Second International Symposium on Quantum Confinement Physics and applications, Vol. 94-17,* pp. 408, 419.

74. Eightfold-coordinated Ba^{+2} has an ionic radius of 1,42Å, whiel Pr^{+3} had a radius of 1.13Å, almost the same as Ca^{+2}(1.12Å), which is known to replace Ba^{+2} suggesting that an ionic radius of 1.12Å is large enough for bonding).

75. Z. Fisk, J. D. Thompson, E. Zirngiebl, J. L. Smith, adn S. W. Cheong, *Solid State Commun. 62,* (1987) 743.

76. The degradation of the superconductivity in (rare-earth)$Ba_2Cu_3O_x$ systems by Ce, Pr, Nd, Cm, and Gd, all of which are magnetic (J=/=0) in the +3 charge state, but not nonmagnetic (J=0) La, proves the magnetic character of the degradation.

77. P. Karen, H. Fjellvag, O. Braaten. A. Kjekshus, and H. Bratsberg, *Acta Chem. Scand. 44,* (1990) 994.

78. C. Infante, M. K. El Mously, R. Dayal, M. Husain, S. A. Siddiqi, and P. Ganguly, *Physica C 167,* (1990) 640.

79. W. B. Yelon private cpmmunication.

80. T. Wada, N. Suzuki, A. Maeda, Y. Yabe, K. Uchinokura, S. Uchida, and S. Tanaka, *Phys. Rev. B 39,* (1989) 9126.

81. W. E. Pickett,*Rev. Mod. Phys. 61.* (1989) 433.